Organometallic Science
https://www.sciltp.com/journals/os

Review

Nano Gold: From Nanoparticles to Atomically Precise Nanoclusters †

Huili Wang, Jean-Luc Pozzo and Didier Astruc *

ISM, UMR CNRS N°5255, Université de Bordeaux, 351 Cours de la Libération, 33405 Talence Cedex, France
* Correspondence: didier.astruc@u-bordeaux.fr
† This review article is dedicated to the memory of Professor Masatake Haruta (1947–2022), a creative and distinguished colleague and friend.

How To Cite: Wang, H.; Pozzo, J.-L.; Astruc, D. Nano Gold: From Nanoparticles to Atomically Precise Nanoclusters. *Organometallic Science* **2025**, *1*(1), 3.

Received: 25 September 2025
Revised: 14 November 2025
Accepted: 18 November 2025
Published: 4 December 2025

Abstract: Gold nanoparticles (AuNPs), with size between 3 and 100 nm are well-known for their optical properties due to their plasmon band related to the resonance of the collective oscillation of their surface electron cloud matching the incident light wavelength. When the AuNPs are smaller than 2.3 nm, they are no longer plasmonic with fcc structures, but they fall in a quantum size regime of ultra-small AuNPs with specific structural, electronic, optical and catalytic properties resulting from molecular diagrams. They are atomically precise nanoclusters (APNCs), and their construction usually follows the Mackay maximum compacity with successive concentric shells of $(10i^2 + 2)$ atoms, meaning that for $i = 1$, the central Au atom is surrounded by 12 Au atoms Au@Au_{12} in many icosahedral Au_{13} clusters and the second layer ($i = 1$) contains 42 atoms with Au@Au_{12}@Au_{42} in a Au_{55} cluster (Schmid's cluster), etc. The icosahedron is the most frequently observed structure in Au APNCs, but the tetra-, hexa-, deca, icosa- and cubocta-hedron structures are also found, and all these symmetrical structures contribute to the cluster stability, as well as the surface Au-S staples. Since each Au atom contributes its single 6s electron to the non-bonding cluster valence electrons, an exceptional stability is obtained when the total number of non-bonding valence electrons contributing to the clusterification reaches one of the magic numbers 2, 8, 18, 34, 58, 92, 138, … corresponding to closed electron shells, when the compacity is high (quasi-spherical). For instance, the 2-electron Au_3^+ and 8-electron Au_{13}^{5+} cores are named superatom clusters. Many clusters, however, also deviate from this trend. The most common cluster series $[Au_{25}(SR)_{18}]^-$ composed of the 8-electron Au_{13}^{5+} core and 6 $[Au(I)_2(SR)_6]^{2-}$ staples are superatom clusters. Although the size-focusing synthesis of the major groups of APNCs is that of thiolate clusters, whose accurate synthesis was astutely focused by the Jin group, the first 8-electron icosahedral phosphine Au_{13} cluster was predicted 50 years ago, then synthesized by the Mingos group in 1981, and in the 2010s new series of Au APNCs appeared with the alkynyl and carbene [both Bertrand-type and N-Heterocyclic Carbene (NHC)-type]) Au APNCs. All these APNC families present very promising electronic, photophysical and catalytic, (including electrocatalytic and photocatalytic) properties that are now exploited by researchers toward biomedicine and energy conversion processes, as well as those of small AuNPs whose catalytic properties were pioneered by Haruta.

Keywords: gold nanoparticles; gold cluster; superatom; catalysis; atomically precise nanocluster

1. Introduction

Gold nanoparticles (AuNPs), long called colloidal gold until the middle of the 20th century, have become a major field of nanoscience because of their fundamental size-and shape-dependent properties including the quantum size effect as well as for their multiple applications in sensing, biology, nanomedicine, optics, electronics, material science, nanotechnology and catalysis [1]. Nanoparticles are also called clusters, but these two terms are often used by certain scientists for the same nano-objects. In fact, it should be better to reserve the term cluster for nanoparticles that are so-called atomically precise, i.e., whose crystal structure have shown the presence of a unique object, whereas, in nanoparticles, transmission electron microscopy (TEM) and atomic force microscopy (AFM) show a certain distribution (dispersity) around a given mass value, even if this dispersity is small (close to 1). Sometimes, the purification of NPs allows isolating atomically precise clusters. In this tutorial mini-review article, after a short historical background, the properties and application of gold nanoparticles are summarized, then gold nanoclusters (AuNCs) are introduced with the main useful ligands including their syntheses, then their optical and catalytic properties.

2. Brief Historical Background of Gold Nanoparticles

AuNPs [1] have an old tradition of more than two millenia, when they were utilized for esthetic and curative purposes in China, old Egypt and Europe during the Middle Age [2], and their curative properties were still in usage until the beginning of the 20th century [3]. The confinement of gold metal at the nanosize revealed new physical and chemical properties, contrasting with those of robust bulk gold metal, and already noticed and exploited in the antiquity. A fascinating example is the Lycurgus gold cup from the 4th century, with its beautiful light properties (ruby red in transmitted light and green in reflected light, visible in the British Museum in London). The first scientific examination of gold colloids was reported in 1857 by Michael Faraday who investigated their optical properties following their synthesis involving biphasic $HAuCl_4$ reduction by phosphorus. Faraday also noticed light scattering (Tyndall effect) by colloidal gold [4]. Half a century later, in 1908, Mie established the plasmon theory and applied it to AuNPs (*vide infra*) [5]. Since the 1940's s electron microcopy (TEM) became available, then popular from the 1960's to allow a better observation of the size and shape of various AuNPs and assemblies (Figure 1) [1,6,7].

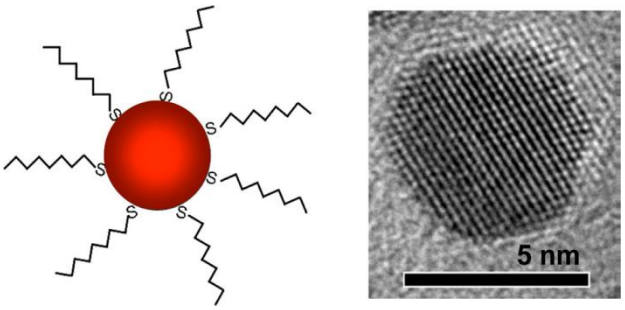

Figure 1. Typical air-stable alkylthiolate (RS) AuNP synthesized upon reduction of $HAu(III)Cl_4$ by alkylthiol (RSH) and in situ reduction by excess $NaBH_4$ of the resulting Au(I)-SR oligomers (see Section 5): structure (**left**, the inner Au atoms are Au(0), whereas the thiolate bonded Au atoms are Au(I)), and Transmission Electron Microscopy (TEM) picture showing the 5-nm Au core (**right**). Reprinted from ref. [7] (Jin's group). Copyright American Chemical Society 2016.

3. Quantum Size-Dependent AuNP Properties

Probably the most important property of AuNPs is their ability absorb and scatter light, which results in a typical wine-red color for small AuNPs, shifting to blue for larger ones. Gold nanoparticles were shown to have properties strongly depending on their size [1]. Below a size of about one to two nm, they are clusters (ultra-small metal nanoparticles) [6–10] that can be rationalized by molecular orbital theory. The capacitance C becomes smaller when the NP size decreases to that of a nanocluster, and when the electrostatic energy $E_{el} = e^2/2C$ becomes larger than the thermal energy kT, Coulomb blockades are observed by cyclic voltammetry [10], for instance in hexanethiol-capped Au_{147} clusters, accommodating here 15 redox states [11] (Figure 2).

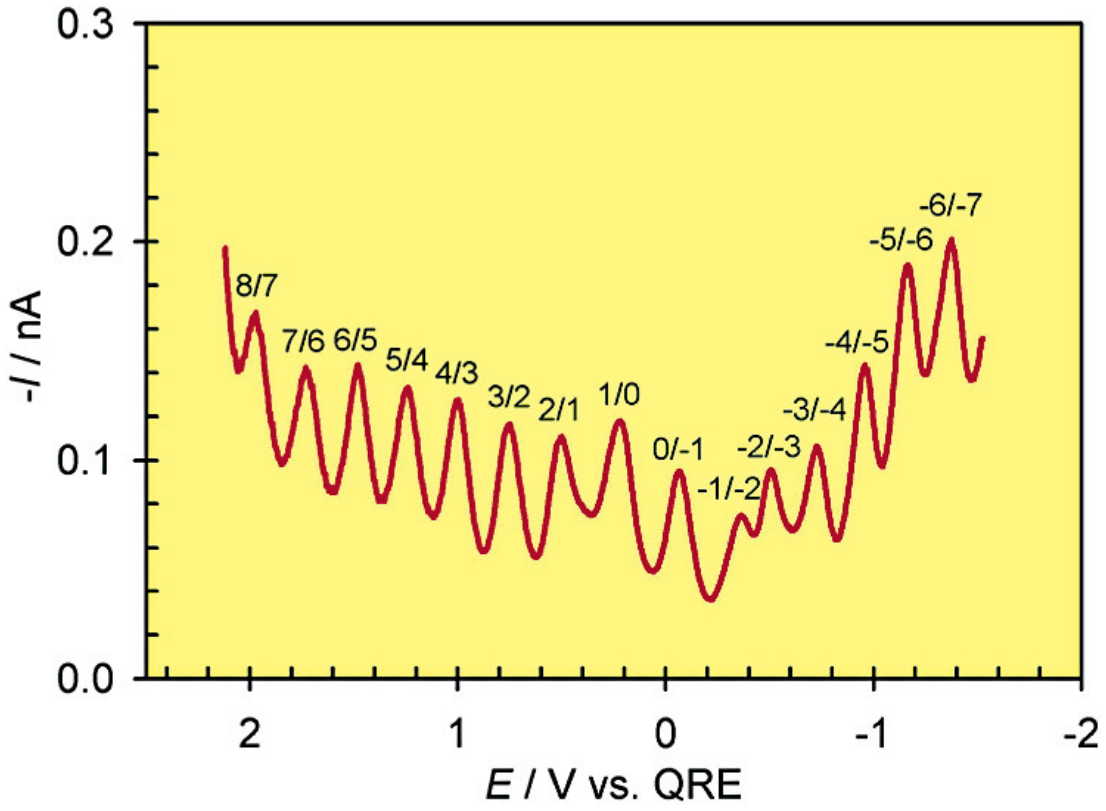

Figure 2. The 15 voltammetric quantized charging peaks for a solution of hexanethiol-capped gold NPs at room temperature for which the variation in peak spacing with increasing charge stored in the NP core is related to the NP capacitance. Reprinted from ref. [11] (Quinn's group). Copyright American Chemical Society 2003.

When the AuNP size reaches that of their valence electron wavelength (around 500 nm; size < 2.3 nm), they behave as zero-dimensional quantum dots relevant to quantum mechanical rules. In these AuNPs, these is a gap between the valence band and the conduction band, unlike in bulk metal. When the surface metal electrons moving freely through the AuNP surface undergo a collective oscillation, the frequency is characteristic of the surface plasmon resonance (SPR) that is observed upon visible light irradiation. This plasmonic frequency is found around 520 nm for AuNP diameter >2.3 nm, and it strongly depends on the size (shifting to 570 nm for 100-nm AuNPs), shape, medium, ligands or adsorbates (sensing), and nature of the plasmonic metal or alloy [1,11–13]. Dark-blue AuNPs of at least 40 nm are observable using a microscope or even naked eye at sufficient concentration. The color of the AuNPs also depends on the solvent refractive index and of nanomaterial coating [1].

4. Recent Plasmonic Sensing Applications of AuNPs

These optical properties of AuNPs led to considerable applications in biomedical sensing [14,15], detection of mismatched DNA [16], cancer cell imaging and photothermal therapy [17–19]. Biosensors [14,20], frequently utilized for convenient bioassays in the fields of healthcare and agriculture [21] are often based on the optical properties, in particular plasmonic of gold and silver nanoparticles, including Surface Plasmon Resonance (SPR) [22,23], Surface Enhanced Raman Scattering (SERS) [24] and Long-Range Surface Plasmon Polariton (LRSSPP) [25]. In these techniques, AuNPs and AgNPs are essential toward biosensors due to their enhancement of SERS and SPR signals. For instance, DNA-functionalized AuNPs allow detecting the RNA sequence [26]. The LSPR detection platform is also offering large possibilities of portable sensor technology with a crucial function in detecting different cancers, fungal and viral diseases, bacterial infection, and cardiac malfunctions. Likewise, in the environmental field, LSPR can monitor food safety and water impurities [27–29].

5. The synthesis of Thiolate AuNPs

Tetrachloroauric acid ($HAuCl_4$), produced by oxidation of bulk gold using *aqua regia* (known from at least a millennium and probably longer) is at the basis of all nanogold syntheses. The most popular AuNP synthesis is the citrate reduction of $HAuCl_4$ published by Turkevich in 1951 [30] and improved by Frens in 1973 [31]. The initial method provided AuNPs of about 20-nm diameter, whereas improvements involved the control of the sodium citrate: gold ratio for pre-chosen sizes between 16 and 147 nm. This later method is still used when the

need for such large AuNPs is required (in biology). The simultaneous addition of trisodium citrate and an amphiphile surfactant such as a mercaptan was an additional improvement [32]. A variety of ligands can be utilized to stabilize AuNPs, including mostly thiolates, but also phosphines, phosphine oxides, amines, stable carbenes, carboxylates, dithiocarbamates and alkynyls [1,33]. Thiolate-stabilized AuNPs have been and are still very popular, because they are air-stable and can be handled, dissolved in common organic solvents, reprecipitated without irreversible aggregation, and characterized almost like ordinary organic compounds, unlike many other types of AuNPS [33]. Their synthesis was first reported in 1993 by Mulvaney and Giersig using thiols of different chain lengths, and methods for their analysis was disclosed in the same time [34]. A very practical method for their synthesis is the Brust-Schiffrin method, published in 1994, with low to moderate dispersity and controlled size between 1.5 and 5.2 nm [35]. This two-phase (toluene/water) synthesis is inspired from Faraday's biphasic method [4] and uses alcanethiols. The anion $AuCl_4^-$ is transferred to toluene using the tetraoctylammonium bromide salt as the phase-transfer reagent and is reduced as well as the thiol by $NaBH_4$, resulting in immediate color change from yellow to deep brown. With dodecanethiol, the size of the AuNPs varies with a nearly Gaussian distribution between 1 and 3 nm observed by TEM [35]. Heating such AuNPs suspension near the boiling point in the presence of the alkanethiol (method called digestive ripening) significantly reduces the average particle size and polydispersity [36] and also leads to the formation of 2D and 3D AuNP superlattices [37]. The Brust synthesis method was extended to a single-phase synthesis [38], and a certain (limited) proportion of alcanethiolate ligands can be replaced by various functional thiols giving the alcanethiol and functional thiolate-AuNP bonding [39] (Figure 3).

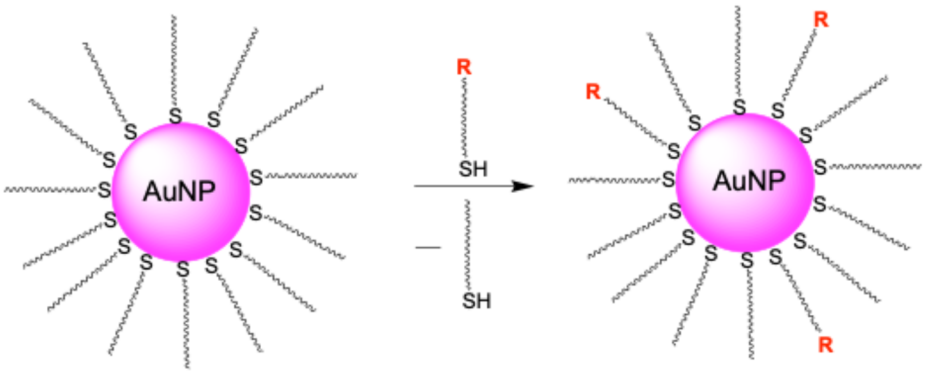

Figure 3. Ligand exchange reaction limited to a proportion of the alkyl thiolate ligands upon reaction with functional thiols (R = Br, OH, CN, CO_2H, anthraquinone, $CH{=}CH_2$, Ar, Fc (Fc = ferrocenyl) [1], in thiolate AuNPs. The reaction proceeds by an associative mechanism, the H atom of the incoming thiol group being transferred to the S atom of the leaving thiolate at the Au core surface. For instance, with R = COFc, the proportion is limited to about 20% [40].

The shapes of AuNPs could be controlled [41], and a variety of AuNPs shapes have been obtained [42], in particular gold nanorods (NRs) with aspect ratios between length and width ranging from 1.5 to 10 synthesized using the seed-mediated growth method [42] and utilized for biosensing and nanodrug delivery [43,44].

6. From Nanoparticles to Atomically Precise Nanoclusters (APNCs)

The world of metal-metal bonds spreads from bimetallic complexes and small, geometrically well-defined clusters (trinuclear, tetranuclear, etc.) [45] to metal NPs. The synthesis of AuNPs was a formidable venture over the last centuries, and they were obtained by aggregation and stabilization of metal NPs upon reduction of a transition metal salt in the presence of a stabilizing ligand, polymer, dendrimer, oxide, etc. NPs comprise hundreds to thousands of metal atoms. However, given the dispersity of these metal numbers in NPs around a medium number value, scientists have desired to obtain small NPs that would also have only a precise geometry and number of atoms, extending the family of clusters to those having numbers of atoms up to more than 100. This has been made possible by enlarging the family of metal-carbonyl complexes [45] and metal-phosphine complexes, but also by synthesizing very small and ultra-small metal NPs with specific ligands such as thiolates, selenolate, alkynyl and NHC or cyclic amino-alkyl carbene ligands that exhibit quantum size effect with specific electronic and chemical properties. The challenge has consisted in finding ways to purify these small NPs or directing as precisely as possible the synthesis of metal clusters with these ligands, giving rise to the family of atomically precise

nanoclusters (APNCs). The smallest APNCs show defined features like molecules, but above a certain number of atoms around 120 (size: 1.7 nm), they reach this quantum size regime (Figure 4).

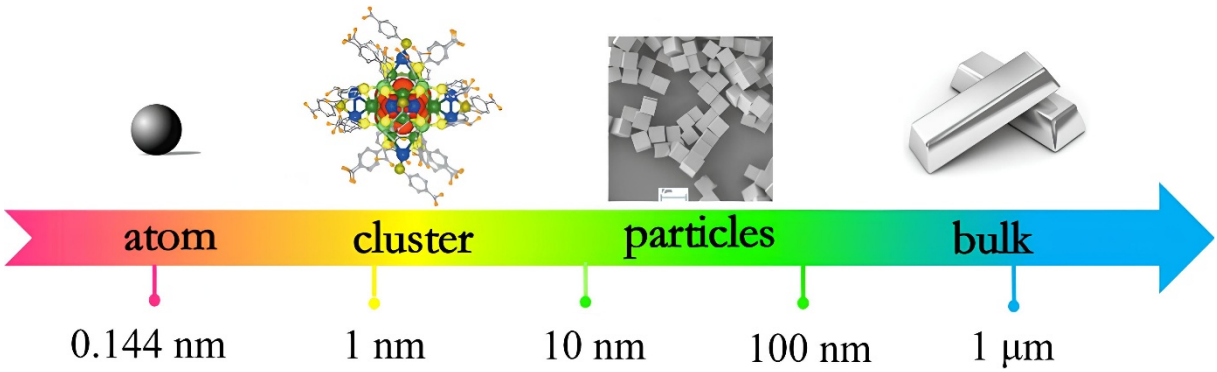

Figure 4. The nanoscale from atom to molecules (<1.7 nm) and quantum sized APNCs (1.7 to 2.3 nm) to nanoparticles (between about 2.3 and 100 nm, plasmonic nanogold) and bulk metal. Reproduced with permission from ref. [8] (groups of Dong and Zang). Copyright 2024 American Chemical Society.

The number of metal atoms *n* per Au APNC (Au_nL_m) in the range of 1–2 nm is about equivalent to a range of *n* from approximately 10 to 250 atoms and can be estimated by *n* = (particle volume, nm^3) × 59 atoms/nm^3, which is derived from face-centered cubic (fcc) gold, and is accurate enough even for non-fcc-structured non-plasmonic Au nanoclusters smaller than 2.3 nm [45].

7. The Syntheses of Atomically Precise Gold Thiolate Nanoclusters (AuNCs)

The AuNP structures lack precision, and the nano-objects are not unique (dispersity), which makes difficult relationships between their structures, functions and properties. On the other hand, atomically precise nanoclusters (APNCs) have long been known since Cotton's cluster definition [46]. For instance, in the well-known and extensively studies metal-carbonyl cluster family, an enormous variety of atomically-precise cluster compounds became available upon easy exchange of the carbonyl ligands by phosphine (mostly) and other ligands, a reaction that was particularly convenient and selective using electron-transfer chain catalysis [47,48].

Since the beginning of the century, however, in continuation of the easily available thiolate AuNPs introduced by the Brust method, the most popular ligands in APNCs have been by far the thiolates [49]. For instance, in an elegant seminal work, Tsukuda's group synthesized, using a modified Brust-Schiffrin method, and separated from their mixture by gel electrophoresis, nine water-soluble Au thiolate APNCs of different sizes, and each of these isolated APNCs was characterized by electrospray ionization-mass spectrometry (ESI-MS) [50]. Matrix-assisted laser desorption/ionization mass spectrometry (MALDI-MS) can also be utilized, but often results in fragmentation of NCs, even under threshold laser intensity. In order to avoid such tedious separations, strategies have been introduced to obtain the most thermodynamically stable Au APNC species from a NC mixture. The Jin group has conducted a careful and useful mechanistic exploration of the controlled syntheses of thiolate Au APNCs. These authors have provided an overview of the efficient strategies for precise thiolate-AuNC preparations and shown the effects of various key parameters on the Au APNC size and composition [7,50]. The formation mechanisms of the APNCs $Au_n(SR)_m$ involve first the generation of intermediate NCs via the reduction of Au(I)-SR complexes, and then the size evolution of intermediate NCs forming Au APNC [45,49,50]. APNCs have been synthesized taking into account several key factors including in particular kinetic control, seeded growth, in situ two-phase ligand exchange, and metal exchange [7].

A decisive step in the selective preparation of Au-thiolate APNCs was Jin's introduction of the "size-focusing" methodology, based on kinetically controlled, thermodynamic selection. This was striking for the synthesis of the central family of Au APNCs, $Au_{25}(SR)_{18}$, involving numerous thiols RSH with R = $-C_2H_4Ph$, $-C_6H_{13}$, $-C_{12}H_{25}$, −glutathione, $-n$-$C_{10}H_{22}COOH$, etc. The first step, reduction of Au(III) by excess thiol leading to the polymeric Au(I)(SR) intermediate, was conducted at 0 °C with very slow stirring (~30 rpm), which was critical to get high-purity Au_{25} $(SR)_{18}$ APNCs (for X-ray crystal structure determinations), and was followed by the reduction by $NaBH_4$ at 0 °C, with fast stirring (1100 rpm), of Au(I)(SR) [50,51] (Figure 5).

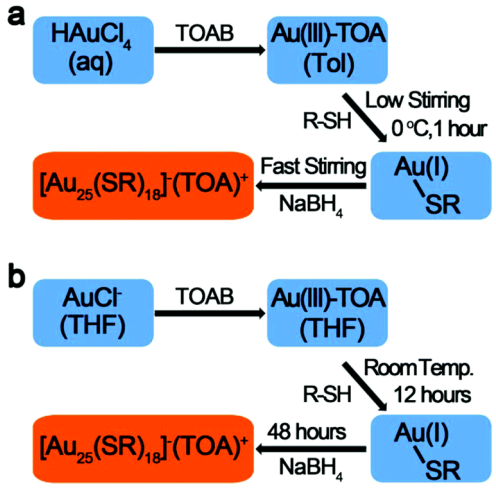

Figure 5. Stepwise synthesis of the clusters $[Au_{25}(SR)_{18}]^{-}[TOA]^{+}$; (**a**,**b**) refer to different solvent conditions. The intermediate Au(I)SR species are oligomers. Reprinted from ref. [52] (Zhu's group). TOAB = tetraoctylammonium bromide. Copyright Royal Society of Chemistry 2018.

These particular clusters are characterized in UV-vis. spectroscopy by three absorption bands at 670, 450, and 400 nm [50,51]. Jin's group extended the size-focusing methodology to other Au-thiolate APNC such as $Au_{38}(SR)_{24}$ and $Au_{144}(SR)_{60}$ by utilizing the different stabilities of different sized $Au_n(SR)_m$ NPs and managing a specific size distribution of the starting $Au_n(SR)_m$ mixture down to one size [50]. To date, more than forty Au-thiolate APNCs with Au atom numbers from 18 to 279 have been reported together with their X-ray crystal structures, but the $Au_{25}(SR)_{18}$ family is the most frequently encountered, in particular because it is the most robust and easily prepared [53]. The X-ray crystal structure of $Au_{25}(SR)_{18}$ (R = phenylethyl) was first reported by Zhu et al. in 2008; it exhibits an icosahedral Au_{13} kernel wrapped by six $Au_2(SR)_3$ motifs. The thiolate ligands present sulphur atoms bridging two core gold atoms, forming an extended "staple" motif, in which three sulfur and two gold atoms are arranged in a 'V-shaped' −S−Au(I)−S−Au(I)−S− pattern. The structure is anionic with a tetraoctylammonium cation that was used as phase transfer agent in the synthesis, but it has also been obtained in the neutral form upon aerobic oxidation of the anionic cluster [52,54,55] (Figure 6).

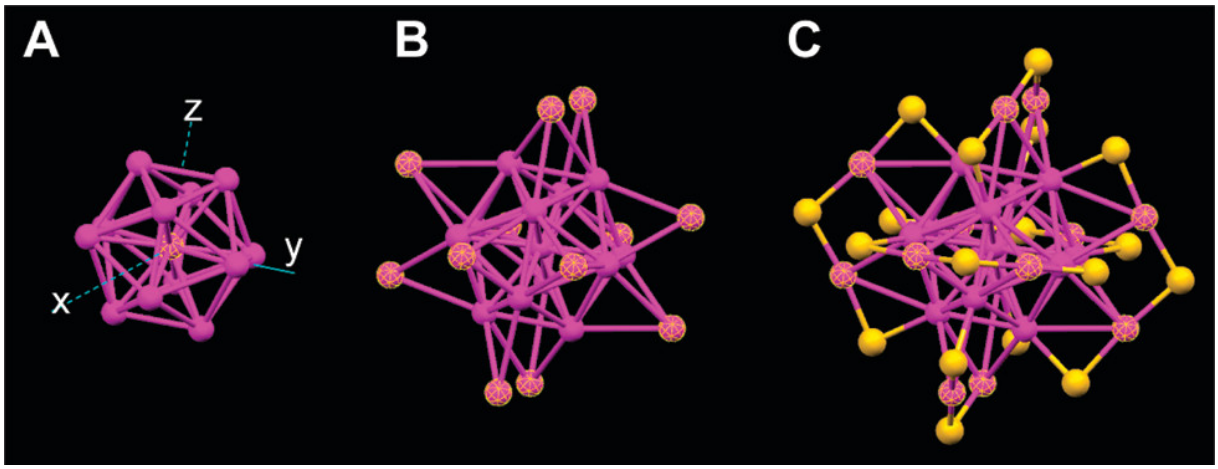

Figure 6. Crystal structure of a $Au_{25}(SR)_{18}$ cluster (R is phenylethyl group): (**A**) the icosahedral Au13 core; (**B**) the Au_{13} core plus the exterior 12 Au atoms; (**C**) the whole Au_{25} cluster protected by 18 thiolate ligands (for clarity, only S was shown, magenta, Au; yellow, S). Reprinted with permission from ref. [54] (Jin's group). Copyright 2008 American Chemical Society.

The size-focusing method was extended to the syntheses of $Au_{64}(SR)_{32}$, $Au_{99}(SR)_{42}$ and $Au_{333}(SR)_{79}$ [7,55]. The next noteworthy Au-thiolate APNC family are $Au_{38}(SR)_{24}$ for which Jin designed, for its synthesis, a two-step method involving first the preparation of a water-soluble capped $Au_x(SG)_y$ (GSH = glutathione) mixture with a *controlled* size distribution, followed by further use for subsequent thermal thiol etching in two phases (water/toluene), $Au_x(SG)_y$ in water and a new thiol in toluene. Prolonged thermal reaction in excess thiol, such as neat dodecanethiol or dilute phenylethanethiol, resulted in gold core etching (involving also O_2), and the initial,

polydisperse $Au_x(SG)_y$ were converted to single-sized $Au_{38}(SR)_{24}$ with high purity in the organic phase [56]. The APNC $Au_{38}(SR)_{24}$ possesses a Au_{23} kernel viewed as two fused Au_{13} icosahedra that share a common Au_3 face (Figure 7) [57]. There are several examples of such fusion of gold kernel complexes into larger clusters [52].

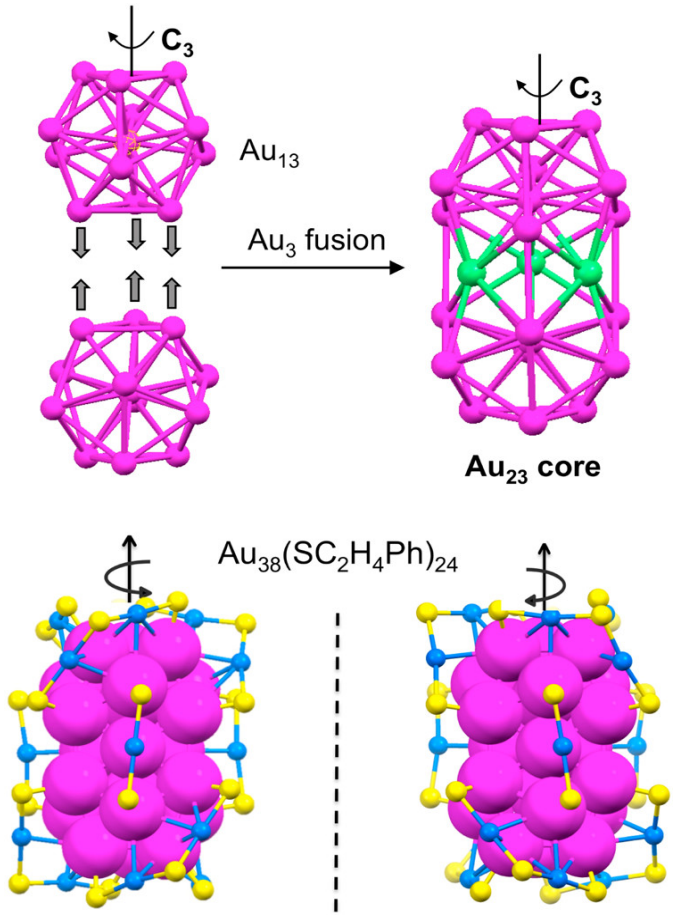

Figure 7. Top: the cluster $Au_{38}(SR)_{24}$ with a Au_{23} kernel represented as two fused Au_{13} icosahedra sharing a Au_3 face and (**bottom**) positions of dimeric staple $Au_2(SR)_3$. Bottom: monomeric staple $Au(SR)_2$ on the kernel, and the two enantiomers. Yellow, sulfur; blue and purple, Au. The carbon tails ($-SC_2H_4Ph$) are omitted for clarity. Reprinted with permission from ref. [57] (Jin's group). Copyright 2010 American Chemical Society.

An impressive review by Zhu and co-workers published in 2018 emphasized the predominance of the $Au_{25}(SR)_{18}$ family and detailed the various synthetic procedures with different thiol ligands and their properties and applications, including the useful water-soluble APNCs [52]. In particular, glutathione-Au APNCs were prepared with many Au nuclearities and were used as intermediate for the syntheses of bioligand-containing thiolates such as for instance cysteine or bovine serum albumin.

In parallel with the Au APNCs, Ag APNCs and many other late transition metal thiolate APNCs have been synthesized, forming a large family of late transition metal thiolate APNCs [7,8,50–62], comparable to the late transition metal carbonyl APNC family [63,64], that also includes Chini's giant metal carbonyl clusters, which were current at the end of the 20th century [65].

8. Superatom Clusters

A superatom cluster is defined as a cluster that has properties similar to those of an atom. Superatom complexes are superatoms clusters containing a metal cluster core stabilized by ligands. In gold cluster complexes, a simple electron counting rule is used providing the total number of non-bonding cluster valence electrons (n_e) corresponding to a so-called magic number: $n_e = N\,v_A - X - z$ where N is the number of metal atoms A in the core, v is their atomic valence, X is the number of electron withdrawing (one-electron) ligands, and z is the overall charge on the complex [66]. This rule parallels the determination of the number of non-bonding metal valence electrons in monometallic complexes ($N = 1$), calculated as $n_e = v_A - X - z$ [64].

In the same way as monometallic metal complexes are often stable when their number of valence electrons $n_v = v_A + X - z + 2$ L (L = 2-electron donor such as phosphine) reaches the magic number of 18 (18-electron "rule"

in transition metal complexes), which corresponds to closed shells, it has been shown that gold clusters reach an exceptional stability when the total number of non-bonding valence electrons contributing to the clusterification reaches one of the magic numbers 2, 8, 18, 34, 58, 92 138, … corresponding to closed electron shells [66,67]. Here, the 2-electron donors such as phosphines are not taken into account in the magic atom number count. The electronic configuration of the gold atom being $(Xe)(4f^{14})(5d^{10})(6s^1)$, each gold atom can contribute its single 6s electron to the cluster. For instance, in the numerous Au_{13} clusters, the 8-electron superatom configuration $(1S)^2(1P)^6$ is reached by 6s(Au) combinations, formally for $[Au_{13}]^{5+}$, in which the average gold oxidation state is intermediate between 0 and I in a pseudo-spherical homogeneous medium (I_h symmetry). Mixtures of chloride, thiolate, phosphine (or diphosphine) and stable carbenes, i.e., NHC carbenes or Bertrand's cyclic (alkyl)(amino) carbenes, are the most frequently encountered sets of ligands in such superatom 8-electron Au_{13} clusters. The icosahedral Au_{13} clusters were predicted 50 years ago by Mingos [68], and the synthesis and crystal structure of the first example, matching the 8e $[Au_{13}]^{5+}$ electronic configuration, $[Au_{13}(PPhMe_2)_{10}Cl_2]$ $(PF_6)_3$, were reported by Mingos' group in 1981 [69]. The synthesis of an Ag_{13} icosahedron cluster is much more recent [70].

In the series of homoleptic Au_{25}-thiolate APNCs, the 8-electron superatom clusters $[Au_{25}(SR)_{18}]^-$ reported with their X-ray crystal structure by the groups of Jin [53] and of Murray [71], and predicted by DFT analysis in 2008 by Grönbeck, are anionic (*vide supra*), and the ground state was described as an icosahedral Au_{13} core protected by six MeS−Au(I)−MeS−Au(I)−MeS units, i.e., $Au_{13}[(MeS)_3Au(I)_2]_6$ (Figure 8). The latter plays a major role in the fluorescence of the $[Au_{25}(SR)_{18}]^-$ clusters due to charge transfer from the ligands to the core (LMNCT), through the Au-S bonds, and electrons density transfer from electron-rich atoms of the ligands to the core [72].

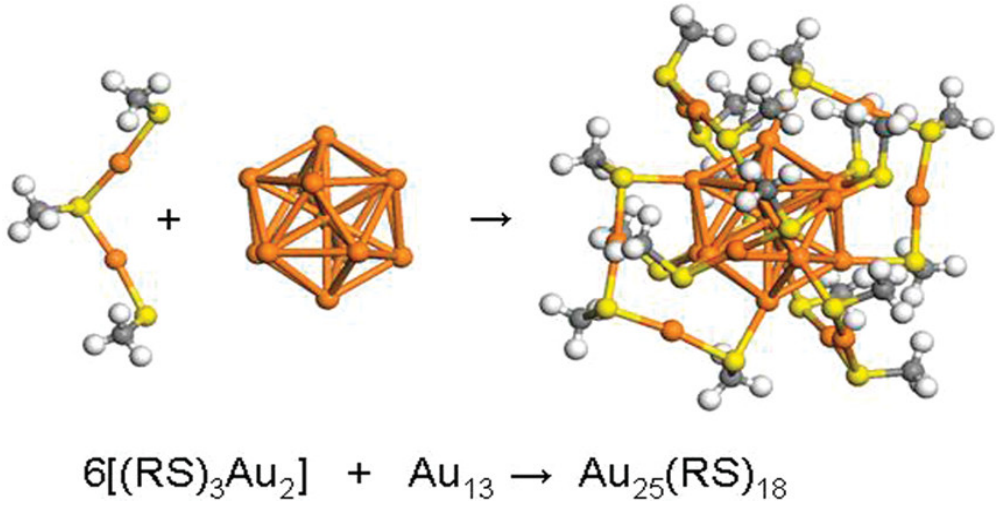

Figure 8. The $[Au_{25}(SR)_{18}]^-$ cluster assemblies of the 8-electron superatom $[Au_{13}]^{5+}$ core and 6 dianionic $[RS{-}Au(I){-}MeS{-}Au(I){-}RS]^{2-}$ staple units (on the figure, R = Me). Reprinted with permission from ref. [73] (groups of Häkkinen and Grönbeck). Copyright 2008 American Chemical Society.

However, with one less thiolate ligand, the neutral 8-electron closed-shell Au_{13} APNC has been reported by Demescence's group with $Au_{25}(SR)_{17}$ [72].

The compacity of a cluster of metal atoms has been shown by Mackay involving successive concentric shells of $(10i^2 + 2)$ atoms [74]. Such optimal compacity close to a sphere is reached in the central $M@M_{12}$ icosahedron, more compact than the cuboctahedron. Upon adding the next concentric shell (i = 2), i.e., M_{42}, a $M@M_{12}@M_{42}$, an assembly of 55 atoms is reached, as first represented by Schmid's iconic $[Au_{55}(PPh_3)_{12}Cl_6]$ (6, *vide infra*). Many stable gold clusters do not correspond to such packing, however. For instance, the first X-ray crystal structure determination of a gold-thiolate APNC was that of the remarkable 58-electron closed-shell cluster Au_{102}(*p*-MBA)$_{44}$ (*p*-MBA = *p*-mercaptobenzoic acid) reported by Kornberg's group in 2007 (58 is one of the magic numbers, vide supra) with a 49-atom Marks decahedron gold core, thus distinct from the Mackay compacity [75] (Figure 9).

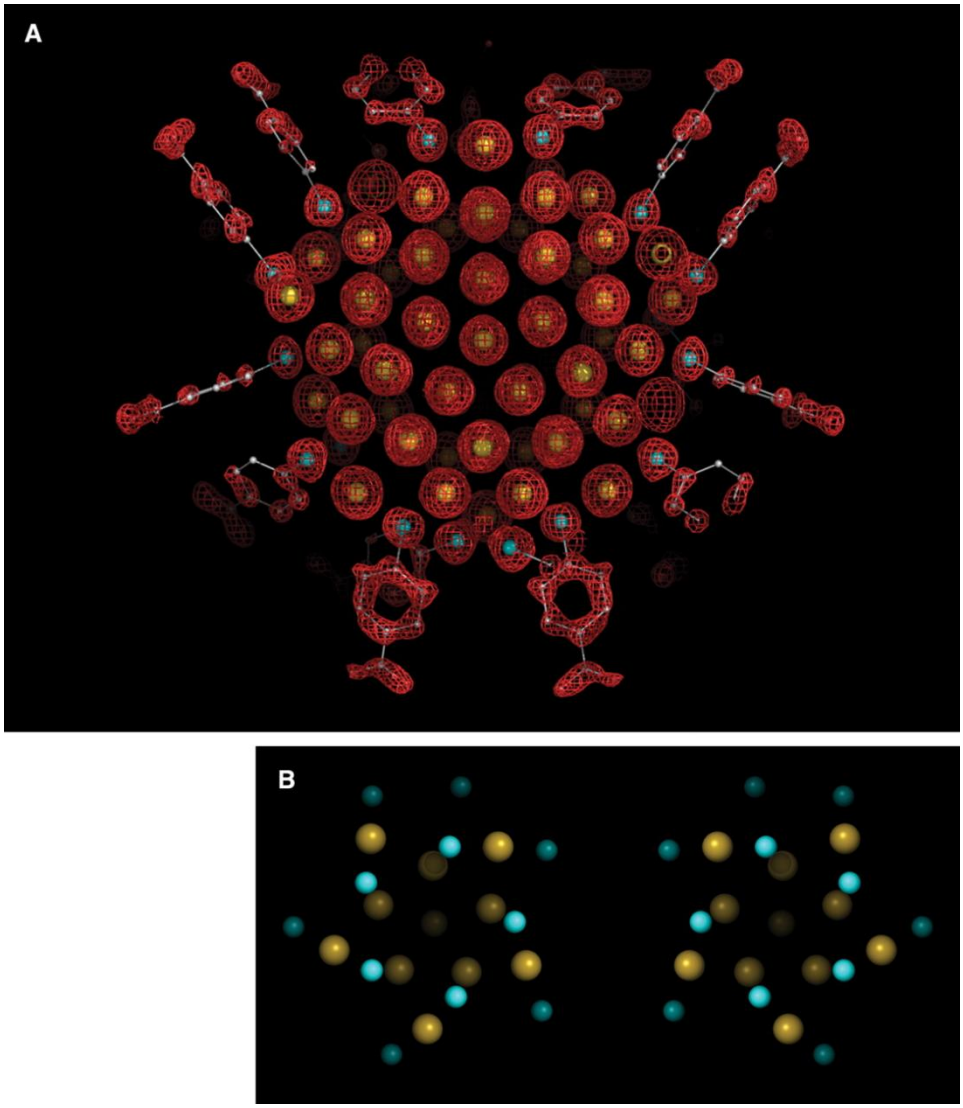

Figure 9. X-ray crystal structure of the Au_{102}(*p*-MBA)$_{44}$ nanocluster. (**A**) Electron density map (red mesh) and atomic structure (Au atoms as yellow spheres, and *p*-MBA as framework and with small spheres [S in cyan, C in gray, and O in red]). (**B**) View down the cluster axis of the two enantiomeric clusters. Color scheme as in (**A**), but only the S atoms of *p*-MBA are shown. Reprinted with permission from ref. [75] (Kornberg' group) Copyright Science 2007.

Progression of the free Au electron number from the 4-electron $[Au_{15}(SR)_{12}]^-$ to 6-electron $[Au_{20}(SR)_{15}]^-$ to 8-electron $[Au_{25}(SR)_{18}]^-$ to 10-electron $[Au_{29}(SR)_{20}]^-$ etc. to 12e → 14e → 16e → 18e → 20e was obtained by Xie's group, characterized using ESI-MS. The Xie group engineered reduction, seed-mediation and assembly methods for ligand exchange and alloying, in particular with Ag, providing a diversity of Au and alloyed APNCs [76,77] (Figure 10). Doping sites of heteroatoms in APNCs $Au_{25}(SR)_{18}$ towards alloying (with Ag, Cu, Pt, Pd, Hg, Cd, and Ir) were also proposed by the Jin and Zhu groups [78].

The advantages in cluster structural precision includes increased optical, photophysical, electronic, and catalytic properties [45–48], as well as promising applications toward chemical and biological sensing, and energy conversion and catalysis applications [52,55–58].

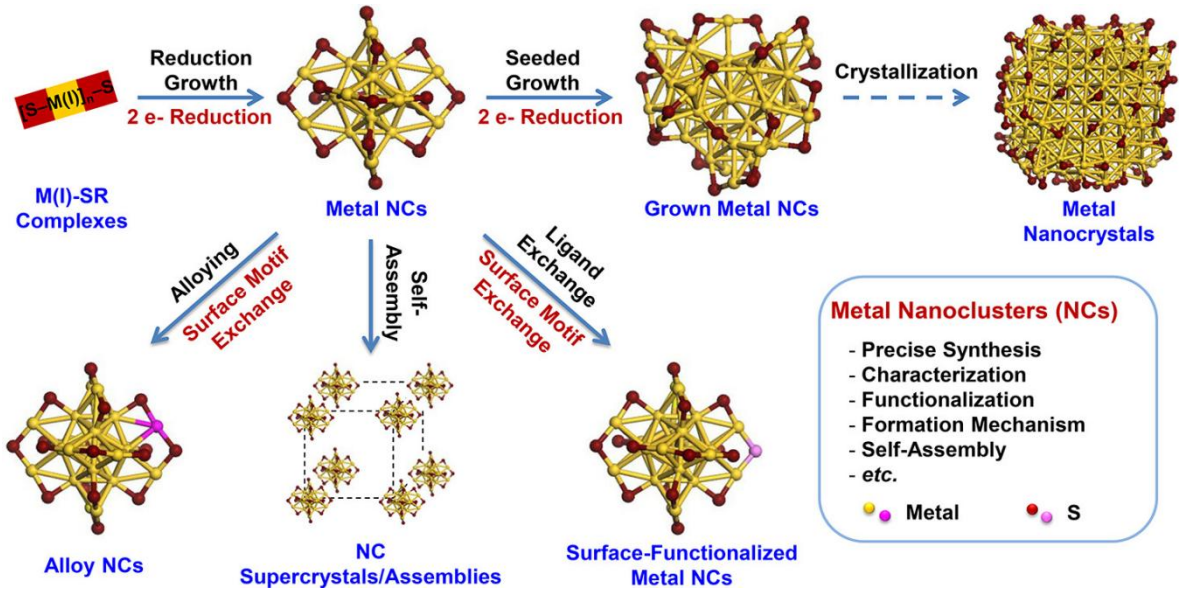

Figure 10. Synthetic routes to metal APNCs: (a → b) preparation of M(I)-SR precursors, (b → c) reduction growth, (c → d) seeded growth, (c → f) alloying reaction, (c → g) ligand exchange reaction, (c → h) self-assembly of APNCs, and (d → e) evolution from the APNCs to nanocrystals. Reprinted with permission from ref. [77] (Xie' group). Copyright Science 2018.

9. Alkynyl-Gold APNCs

The Tsukuda group reported in 2011 the first synthesis of phenylalkynyl-Au clusters by reacting phenylacetylene with AuNPs weakly stabilized by PVP, the alkynyl C-H bond being broken by oxidative addition at the Au(0) NP surface, as shown by the disappearance of this C-H bond of the phenylethynyl-Au clusters in the IR spectrum. The MALDI TOF analysis showed the formation of the different clusters $Au_{43}L_{22}$, $Au_{46}L_{24}$, $Au_{52}L_{26}$, $Au_{54}L_{26}$, $Au_{59}L_{27}$, $Au_{71}L_{32}$, $Au_{90}L_{36}$, $Au_{94}L_{38}$, $Au_{101}L_{38}$, and $Au_{110}L_{40}$, (L = phenylethynyl) [79]. The Tsukuda group next showed by negative ion MALDI mass spectra that the size of the initial Au-PVP and the nature of solvent in the biphasic reaction were crucial for the selectivity, thus the smallest Au:PVP ratio and the use of chloroform–water biphasic conditions selectively yielded $Au_{54}(C_2Ph)_{26}$ [80]. Using precursors with a small Au: PVP ratio (<2 nm), these authors also synthesized $Au_{34}(PA)_{16}$, $Au_{54}(PA)_{26}$, $Au_{30}(EPT)_{13}$, $Au_{35}(EPT)_{18}$, and $Au_{41–43}(EPT)_{21–23}$, (PAH = phenylacetylene, EPTH = ethynyl-phenanthrene), showing by pH drop of the aqueous phase that the mechanism of alkyne C-H bond cleavage was deprotonation and, by EXAFS, that the alkynyl bonding type to the Au surface was either bridging or hollow site (Figures 11 and 12) [81].

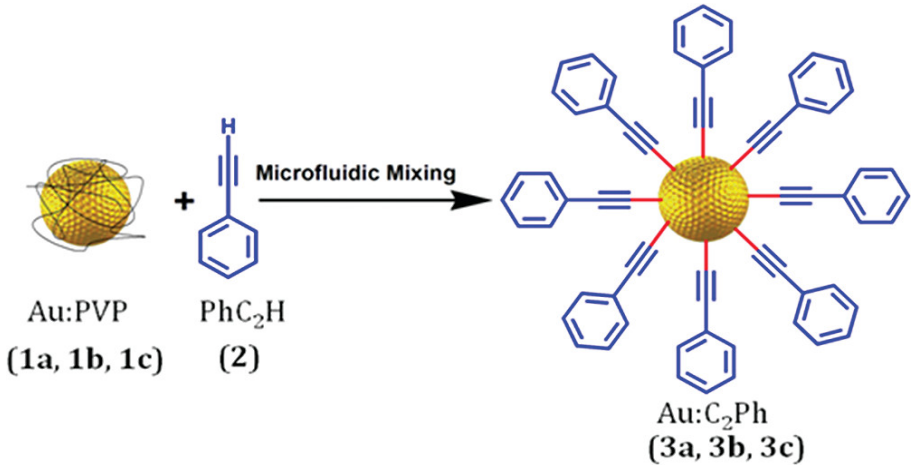

Figure 11. Synthesis of phenylacetylenyl-Au APNC Reprinted with permission from ref. [80] (Tsukuda's group). Copyright American Chemical Society 2011.

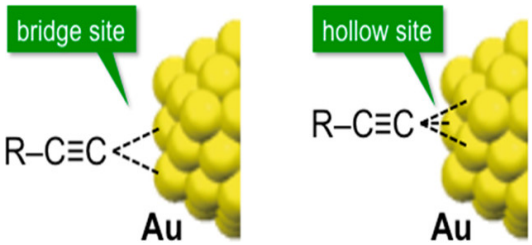

Figure 12. Photoluminescence from the excimer of the ligands and EXAFS analysis of the phenylacetylenyl-Au APNCs showed that the alkynyl group are bonded to the Au core at a briged or hollow Au site. Reprinted with permission from ref. [81] (Tsukuda's group). Copyright American Chemical Society 2013.

The Wang group reported several examples of neutral homoleptic $Au_x(CCR)_y$ APNCs. For instance, direct reduction of PhC≡CAu provided $Au_{44}(PhC{\equiv}C)_{28}$ and $Au_{36}(PhC{\equiv}C)_{24}$ that have fcc-type Au_{36} and Au_{28} kernels, respectively. Remarkably, $Au_{44}(PhC{\equiv}C)_{28}$ was prepared by direct reduction of PhC≡CAu with $NaBH_4$ in $CHCl_3$ [82]. In 2018, the Wang group reported the synthesis and isolation of $Au_{144}(C{\equiv}CAr)_{60}$ (Ar = 2-FC_6H_4-) that possesses a Au_{54} two-shelled Mackay icosahedron (Au_{12}@Au_{42}) enclosed by a Au_{60} anti-Mackay icosahedral shell. The Au_{114} kernel is enwrapped by 30 linear ArC≡C-Au-C≡CAr staple motifs (Figure 13). The preparation of this APNC was conducted by direct reduction involving the precursor Au/dpa (Hdpa = 2,2′-dipyridylamine) that was further mixed with ArC≡CH, Ph_4PCl, and trimethylamine, before dropwise addition of an ethanol solution of $NaBH_4$ [83].

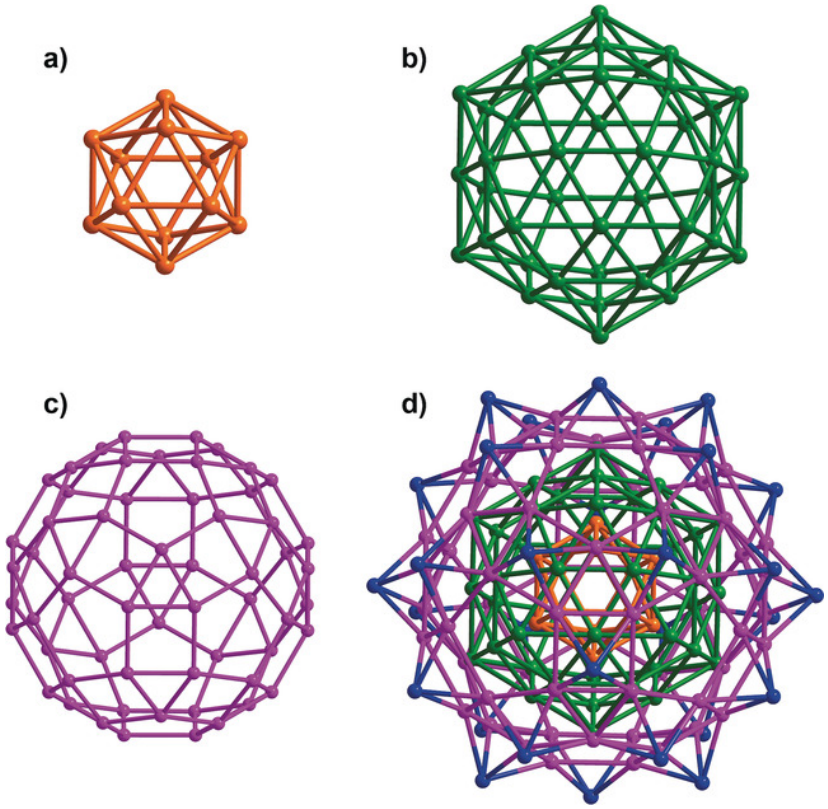

Figure 13. Au_{144} kernel structure in Au_{144} $(C{\equiv}CAr)_{60}$ (Ar=2-FC_6H_4-). (**a**) Innermost shell: Au_{12} Mackay icosahedron (orange). (**b**) Second shell: Au_{42} Mackay icosahedron (green). (**c**) Third shell: Au_{60} anti-Mackay icosahedron (purple). (**d**) Overall Au_{144} kernel structure, with the outmost shell (Au_{30}) highlighted in blue. Reprinted with permission from ref. [83] (Wang's group). Copyright VCH-Wiley 2018.

Alkynyl ligands have versatile coordinating abilities, and the alkynyl triple bond can coordinate to metal centers in σ or/and π modes, including linear, L-shaped, and V-shaped staple motifs, as confirmed by X-ray structural determinations, particularly in bimetallic AuAg APNCs, a variety of other coinage APNCs and in such clusters with mixtures of ligands (chloro or phosphine in addition to alkynyls) (Figure 14) [84–89].

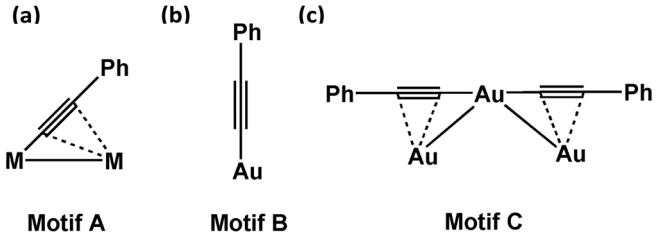

Figure 14. (**a**) Alkynyl–metal interfacial binding model with σ and π interactions; (**b**) alkynyl–gold terminal σ bonding; (**c**) PhC≡C–Au–C≡CPh staple motif on the gold surface. Reprinted with permission from ref. [84] (Wang's group). Copyright Royal Society of Chemistry 2018.

10. Gold APNCs Based on *N*-heterocyclic Carbene (NHC) or Cyclic (alkyl)(amino)carbene (CAAC)

N-heterocyclic carbenes (NHC) and cyclic (alkyl)(amino)carbene (CAAC) are among the most powerful σ-donors. They coordinate to metals in a fashion somewhat similar to phosphines, at least as far as both phosphine and NHC are two-electron (L) ligands that do not oxidize the metal to which they are bonded, unlike the thiolate and alkynyl that are covalently metal-bonded one-electron (X) ligands [90]. The first NHC-Au cluster was reported by Zhou and Chen in 2007 as an intensively luminescent square-planar tetrametallic-cored cluster [91]. This was followed by the finding by Vignole and Tilley of AuNHC superlattices formed by hydridic reduction of the Au-NHC monomer containing $C_{14}H_{29}$ N-alkyl chains [92]. Later, Roesky's group reported heterohexanuclear phosphorescent NHC alkynyl Au-Ag and Au-Cu APNCs [93]. Hexanuclear gold clusters that are particularly stable are the fluorescent C@Au_6 clusters, first introduced by Schmidbauer's group [94,95]. Shionoya first reported the green luminescent NHC–C@Au_6 clusters (Figure 15) [96,97].

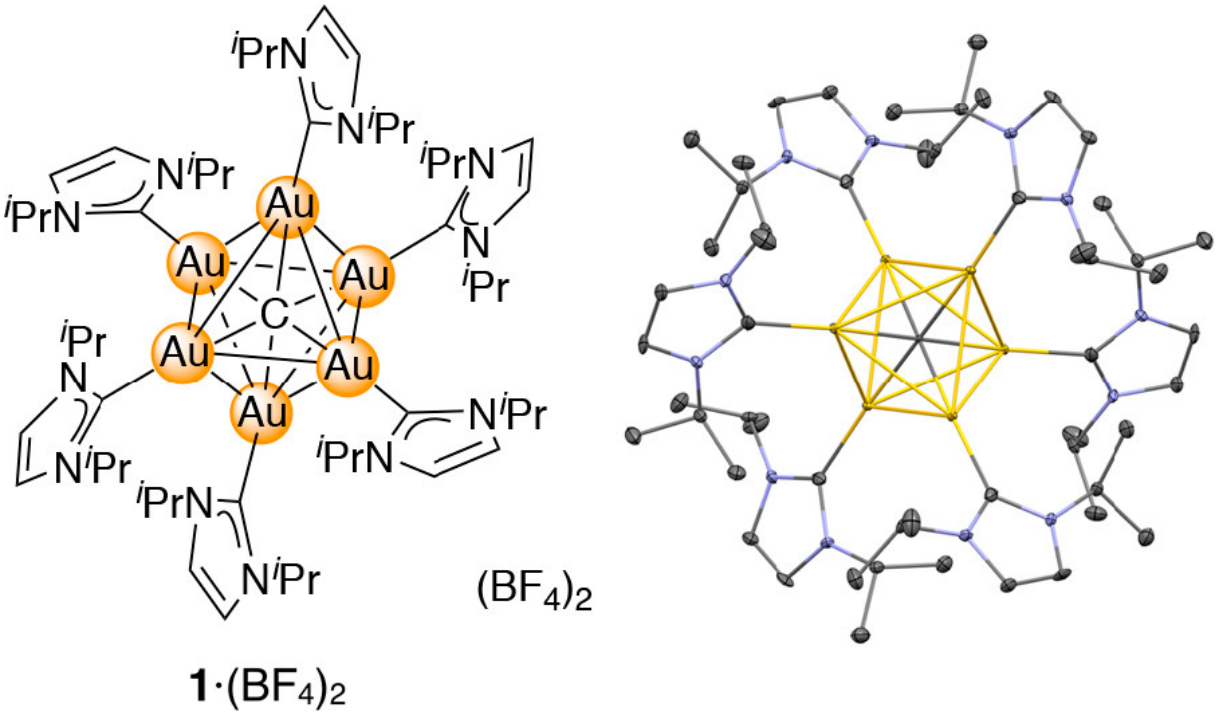

Figure 15. The green luminescent NHC–C@Au_6 clusters. Reprinted with permission from ref. [96] (Shionoya's group). Copyright American Chemical Society 2018.

The luminescence emission was observed at a longer wavelength (λ_{em} 544 nm) than in the PPh_3-C@Au^I_6 cluster (λ_{em} 537 nm), in accord with emission energy correlating inversely with the Au–Au distance, due to the strong σ-coordinating ability of the NHC ligands. DFT calculations confirmed this trend [98].

In the beginning of the 2010's, the groups of Sadighi [99] and Guy Bertrand [100] reported remarkable triangular cationic 2-electron superatom carbene-stabilized $(AuL)_3^+$ clusters with L = *i*-Pr-NHC and cyclic (alkyl)(amino)carbene, respectively, that are considered isolobal to H_3^+. In 2019, several groups reported direct reduction of various NHC-AuCl complexes (available by reaction of Au–Cl(Me_2S) with benzimidazolium chloride salts and K_2CO_3 in Me_2CO at 60 °C) by $NaBH_4$ at 0 °C, followed by annealing with concentrated HCl [101–104].

Herewith, stable robust 8-electron superatom clusters $[Au_{13}(NHC^{Bn})_9Cl_3]^{2+}$ were obtained (NHC substituents: Bn (CH_2Ph), also CH_2Np, CH_2(3-Me-C_6H_4), CH_2(4-Me-C_6H_4)) [101,103] or CH_2py [104].

The thermally and air-stable 8-electron superatom cluster $[Au_{25}(^iPr_2\text{-bimy})_{10}Br_7]^{2+}$ (^{i}Pr-bimy = 1,3-diisopropylbenzimidazolin-2-ylidene), described as two centered Au_{13} icosahedra sharing a vertex, was synthesized upon coreduction by $NaBH_4$ of $^{i\text{Pr}}$NHC−Au−Br (**28**) and Me_2S−Au−Cl [102] (Figure 16).

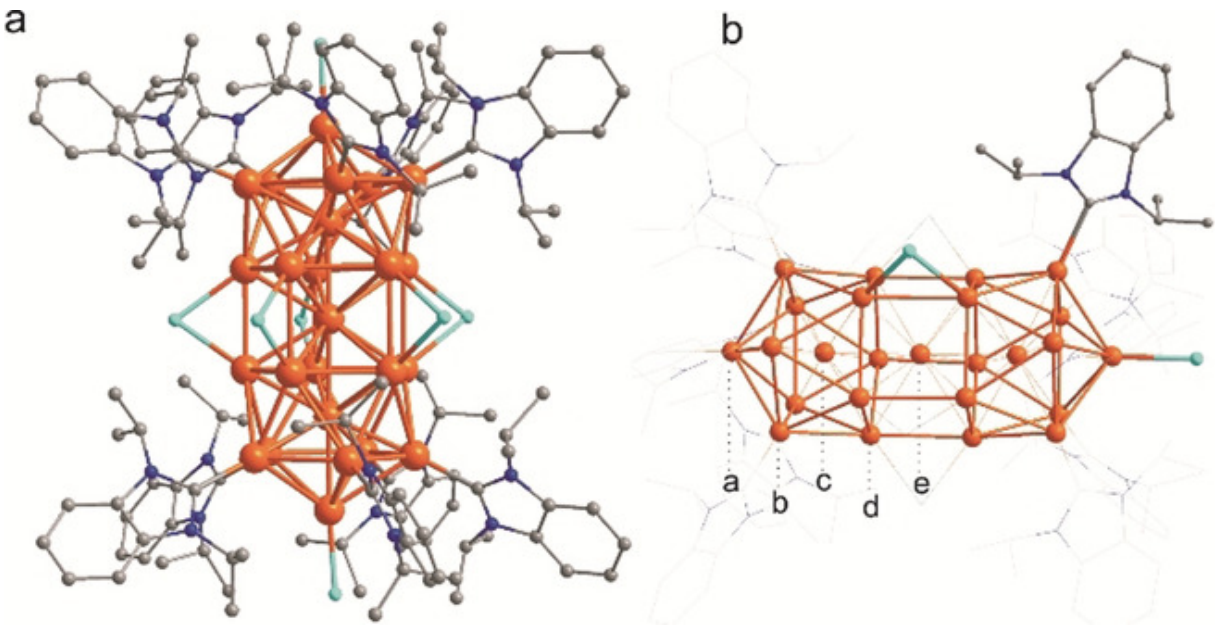

Figure 16. Crystal structure of $[Au_{25}(^iPr_2\text{-bimy})_{10}Br_7]^{2+}$. (**a**) Overall structure and (**b**) Au_{25} metal core showing the binding modes between Au atoms and the ligands (one of each is highlighted). Au orange, Br cyan, N blue, C gray. H atoms are omitted for clarity. Reprinted with permission from ref. [102] (groups of Häkkinen and Zheng). Copyright Wiley-VCH 2019.

For all these NHC-stabilized gold nanoclusters, the structures were ascertained by X-ray crystal structure, ES mass spectrometry, optical data, and XPS. DFT calculations conducted by the Häkkinen group allowed determination of the full cluster electronic structures [40,103–199]. In particular, HOMO–LUMO gaps computed with DFT around 2 eV, confirming spectroscopic data, are in accord with the high cluster stabilities due to the presence of the NHC ligands. Recently, a simpler approach to NHC-gold clusters has been proposed using direct reduction of gold ion and imidazolium salts, as follows, avoiding the isolation of the free carbene [105] (Figure 17):

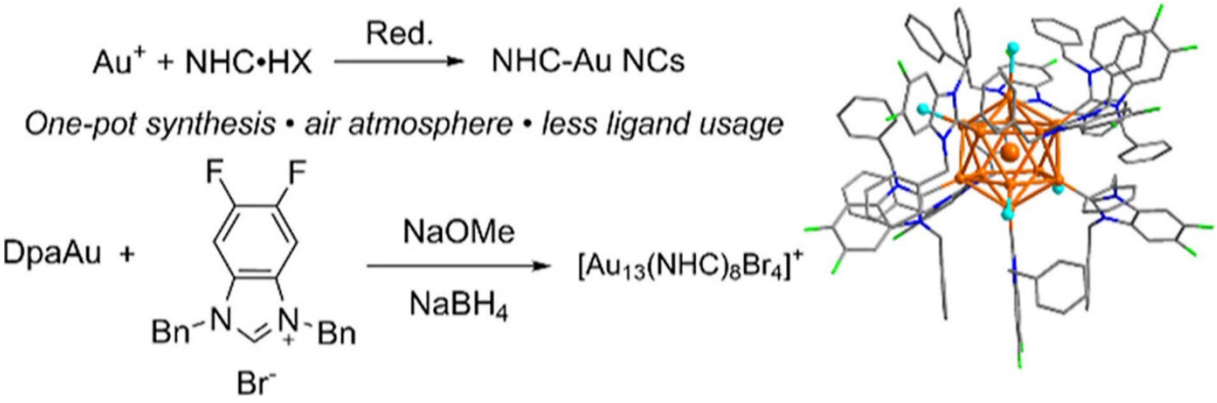

Figure 17. Direct reduction of Au ions and imidazolium salts as a simple synthetic approach to NHC-gold APNCs avoiding the isolation of the free carbenes. Reprinted with permission from ref. [105] (groups of Cholumen, Guo, and Shen). Copyright American Chemical Society 2023.

11. Phosphines

Phosphines share with carbene the two-electron L donor character of the ligands. Gold-phosphine clusters are long known since the report by McPartlin, Mason and Malatesta of the cluster $Au_{11}(PPh_3)_7(SCN)_3$ [106,107]. Mingos' work was crucial in gold cluster chemistry, including especially with molecular orbital calculations [66,108,109]. With gold-phosphine clusters, Mingos showed the hybridization of gold orbitals promoted by the phosphine-Au linear bonding and the versatility of the gold core structure with minute change in the phosphine [109]. Gold–phosphine clusters have been synthesized for instance by direct chemical reduction of Au(I) precursors, in particular $Au(PPh_3)Cl$, and they are readily purified and crystallized, which sharply contrasts with thiolate-gold and other anionic-ligand-gold clusters. Phenyl groups in the phosphine, such as in PPh_3, facilitate crystallization due to the CH–π interaction. The gold cluster structure obtained depends on the reductant/gold ratio, and nature of phosphine, reductant and Au(I) precusor, particularly its anionic ligand, although $HAu(III)Cl_4$ is also sometimes utilized as precursor. The use of strong reductants, such as, typically, $NaBH_4$, lead to the fast formation of large clusters needing purification, whereas weak reductants involving slow reduction lead to monodisperse clusters, but the steric effect also plays a crucial role [110–112].

The Au-phosphine bonding is much weaker than metal-ionic ligand bonds such as Au-thiolate, which makes gold-phosphine clusters excellent candidate for ligand exchange with other useful ligands [111] and in catalysis to liberate potential catalytic metal sites on the gold core surface [113]. Electrospray ionization (ESI) mass spectrometry of positively charged clusters is currently used for the analysis of phosphine gold APNCs, because it produces only little fragmentation. The overall positive charge of clusters allows easy determination by ESI-MS in positive-ion mode, showing mass-to-charge ratio [109]. Collision-induced dissociation (CID) mass spectrometry allows investigating the relative binding energy of ligands to gold, for instance: $PMe_3 < PPhMe_2 < PPh_2Me < PPh_3 < PPh_2Cy < PPhCy_2 < PCy_3$ [14].

Gold–phosphine clusters are often fluxional, i.e., the phosphine ligands rapidly jump from one surface gold metal to the next one via intermediary bridging positions, and the energy barrier between different cluster configurations is low. Such fluxionality is conveniently studied by variable temperature ^{31}P NMR spectroscopy [107].

An illustrious example of large gold-phosphine cluster is that of Schmid's cluster $Au_{55}(PPh_3)_{12}Cl_6$, synthesized in 1981 [114,115], but whose structure was only firmly established in 2015 by aberration-corrected scanning tunneling electron microscopy [116]. Another noteworthy structure that remained uncertain during 45 years is that of the Au_{11} cluster, also with PPh_3 and chloro ligands, because of the formation of stereoisomers, finally determined in 2013 by Simon's group who also considerably contributed to the field [117–119] (Figures 18 and 19).

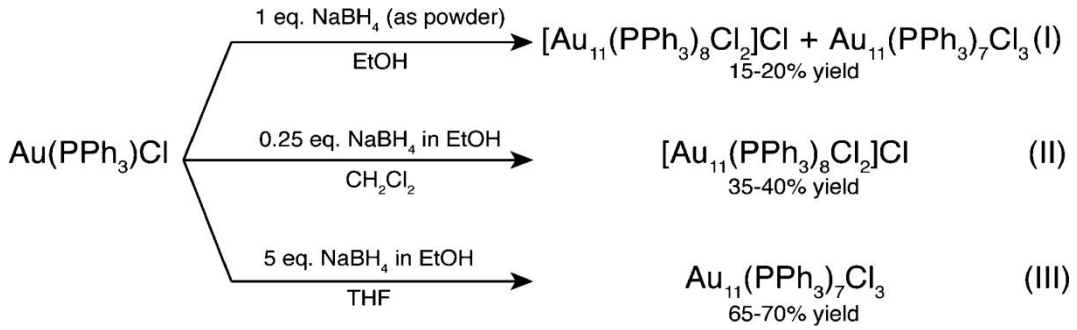

Figure 18. Different syntheses of $[Au_{11}(PPh_3)_8Cl_2]Cl$ and $Au_{11}(PPh_3)_7Cl_3$ compared to the preparation typically used to synthesize Au_{11} [119]. Reprinted with permission from ref. [120] (Hutchison 's group). Copyright American Chemical Society 2023.

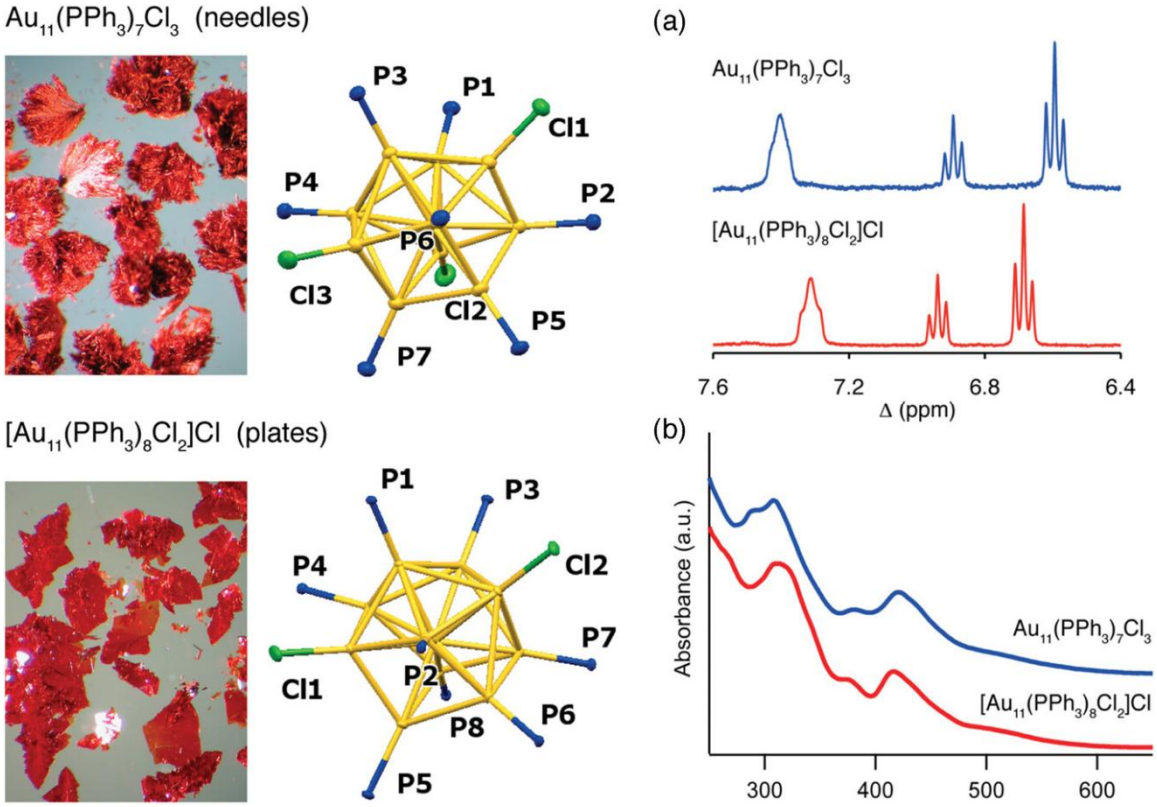

Figure 19. (a) $Au_{11}(PPh_3)_7Cl_3$ **(b)** $[Au_{11}(PPh_3)_8Cl_2]Cl$. Optical micrographs and X-ray crystal structures of the central cores of the two crystalline forms of triphenylphosphine-stabilized undecagold. The needles (top) (a) are composed of undecagold with seven phosphines in the ligand shell: $Au_{11}(PPh_3)_7Cl_3$. The plates (bottom) (b) have been identified as undecagold with eight phosphines in the ligand shell and one outer sphere chloride: $[Au_{11}(PPh_3)_8Cl_2]Cl$. ^1H NMR and UV–visible spectra for the two pure triphenylphosphine-stabilized undecagold clusters recorded in CD_2Cl_2 and CH_2Cl_2, respectively. Optical spectra reported for TPP-stabilized undecagold clusters illustrating clear differences in peak positions. Reprinted with permission from ref. [120] (Hutchison 's group). Copyright American Chemical Society 2014.

12. Compared Properties of Gold APNCs as a Function of Different Ligands

12.1. Thermal and Aerobic Stability and Reactivity

Thiolated Au NCs are remarkable stable, more so than other coinage APNCs (Au > Ag Cu). The stability trend follows that of the core-ligand bond strength (Au–SR > Au–phosphine > Au–amine > Au–citrate). Therefore, the facile triarylphosphine substitution in APNCs is useful in catalysis, *vide infra* [121,122], contrasting with the more problematic usage of more difficult thiolate ligand substitution in catalysis. Magic-electron number closed-shell APNCs, such as, for instance $Au_{25}(SR)_{18}$, are usually more stable than others (ligands being otherwise identical). These APNCs are stable up to 200 °C and progressively lose their ligands above this temperature. In air, the salts of the anion $[Au_{25}(SR)_{18}]^-$ are oxidized to the isostructural neutral cluster. Selective ligand exchange reactions are known to proceed by an associative mechanism in thiolated-Au APNCs like for thiolated AuNPs (Au-SR + R'SH → AuSR' + RSH), and Aikens and co-workers proposed that the most favorable ligand exchange takes place between terminal —SH units and staple gold atoms [123]. In general, the most exposed Au atoms are most susceptible to undergo ligand exchange [124].

Au NCs can be doped by other metal atoms (Pd, Pt, Ag, and Cu), most frequently Ag, by ideally introducing one or a precise number of other metal atoms without changing the APNC core structure. This has been achieved in particular with the robust Au_{25} core of $Au_{25}(SCH_2CH_2Ph)_{18}^-$ providing $Au_{25-x}Ag_x(SCH_2CH_2Ph)_{18}^-$. Doping atoms are most frequently distributed in the surface layer of the cluster, very significantly modifying optic, electronic and catalytic properties [125]. Atomic exchange was recently shown to be interfacial even upon antigalvanic reactions [126] (Figures 20 and 21). Finaly, exchange of the glutathione (SG) ligands in$Au_{25}(SG)_{18}^-$ with functional SG is a valuable method to obtain functionalized APNCs possessing rich properties [127].

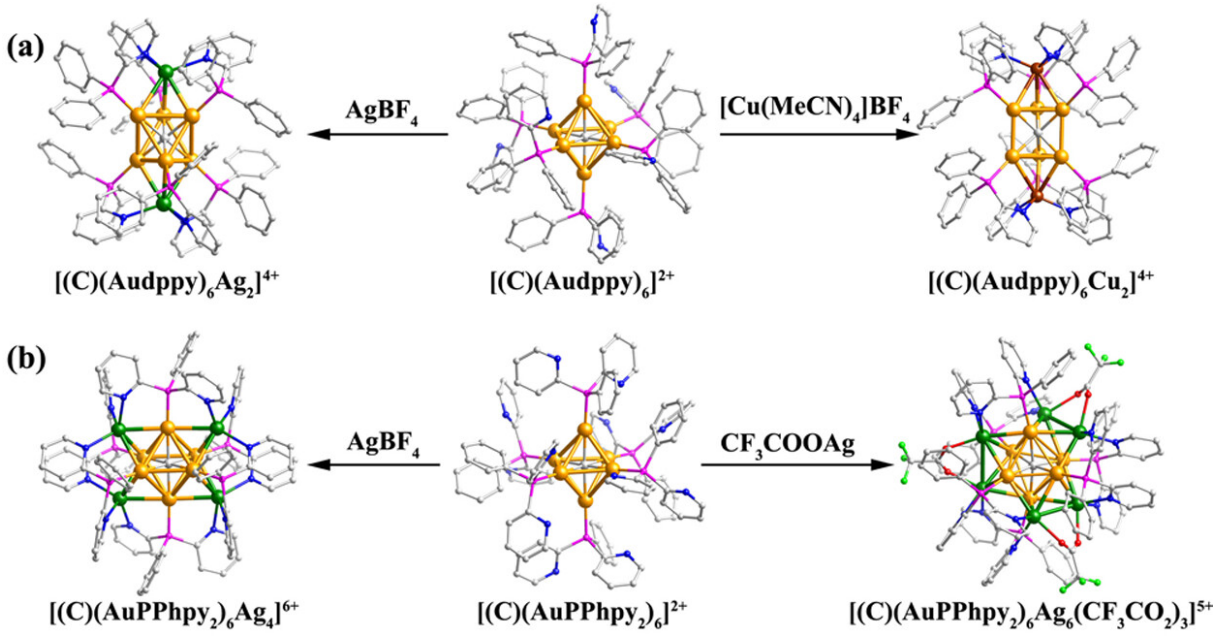

Figure 20. (a) $[(C)(Audppy)_6]^{2+}$; **(b)** $[(C)(AuPPhpy_2)_6]^{2+}$. Examples of metal doping of Au APNCs with the other plasmonic metals. Reprinted with permission from ref. [8] (Dong and Zang group). Copyright American Chemical Society 2014.

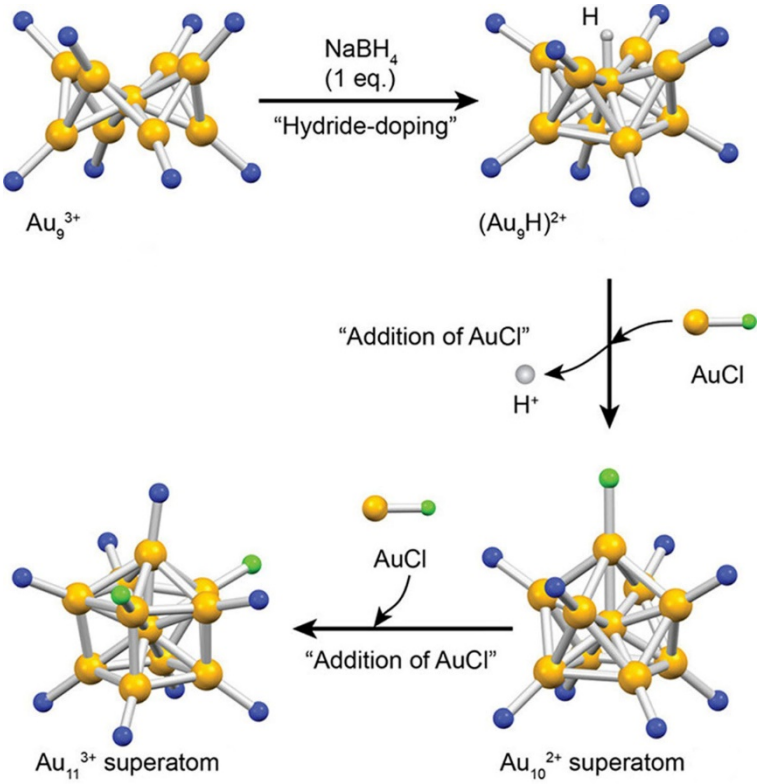

Figure 21. Tsukuda's hydride doping of the 6-electron cluster $[Au_9]^{3+}$ yielding the 6-electron cluster $[Au_9H]^{2+}$. Only the bottom structures are super atoms. Adapted with permission from ref. [128] (Tsukuda's group). Copyright American Chemical Society 2014.

12.2. Ligand Exchange in Gold APNCs

Contrary to carbonyl APNCs in which the electron-transfer chain catalysis technique allows clean single carbonyl exchange by phosphines [46,47], ligand exchange in other APNCs containing phosphines, thiolates, selenate, carbene ligand cannot occur so simply without structural rearrangement of the cluster core without change of the number of metal atoms. For instance, with water-soluble Au-SG cluster mixtures (GSH = glutathione),

reaction with GSH in water provides restructurations of the various Au cores (a process called etching), ultimately yielding the most robust $Au_{25}(SG)_{18}$ nanocluster. Further ligand exchange with other thiols such as *N*-acetyl- and *N*-formyl-glutathione were complete, yielding $Au_{25}(SG)_{18}$ nanoclusters functionalized with these thiols without restructuration, *vide supra* [127]. A general method of syntheses of $Au_{25}(SG)_{18}$ nanoclusters was provided in Pradeep's review [9].

Phosphine ligands can be readily exchanged either by other phosphines, diphosphines or carbenes that are L (or L_2) ligands or by anionic X ligands by reactions with thiols, the resulting thiolates being much stronger ligands than L ligands, in all cases with cluster core restructuration. Yet, this type of reaction has received considerable attention. A very detailed review of the numerous ligand exchange reactions involving a variety of mono-and hetero polymetallic APNCs, in particular those of gold APNCs, has been published by Kang and Zhu [111]. For instance, upon ligand exchange with thiolates, many clusters (but not all) yield the most robust clusters $Au_{25}(SR)_{18}$ [11,52].

12.3. Optical Properties

The plasmon band of AuNPs progressively blue shifts as the AuNP becomes smaller and disappears below around 2 nm when clusters are defined by energy levels and treated by quantum mechanics. Then, the optical spectra and electronic transitions are computed by DFT calculations, first achieved by Christine Aikens for $Au_{25}(SR)_{18}$, reproducing the experimental spectrum [54]. In that case, almost only the atomic orbital contributions of the 13 Au atoms in the icosahedral core compose the HOMO and LUMO, which justifies the view of this cluster as a 8-electron superatom $[Au_{13}]^{5+}$ and produces the 670 nm absorption band. Significant spin–orbit interaction provokes splitting of the superatomic 1P HOMO, responsible for the 800 nm band, as shown by Jiang et al. [129].

The nonlinear optical properties of the main Au NCs, i.e., $Au_{25}(SR)_{18}$ and some high-nuclearity Au NCs two-photon absorption (TPA), two-photon fluorescence (TPF), and second/third harmonic generation (SHG/THG)) could find applications in high-resolution multiphoton imaging [52,130].

12.4. Photoluminescence

Photoluminescence has attracted a lot of attention, because of applications in cell labeling, biosensing, and phototherapy, especially because these nanomaterials are non-toxic and robust, as recently reviewed by Kang and Zhu [112,131]. Time-resolved fluorescence studies showed that the AuNC visible luminescence was due to the metal core, whereas NIR luminescence was due to the —SR—Au(I)—SR—Au(I)—SR—staples [131]. The luminescence is usually weak in Au-thiolated NCs with quantum yield (QY) lower than 20%, emission lifetimes in the nanosecond range, and emission wavelengths above 630 nm (red color). However, luminescence can be enhanced by water-solubilizing, electron-donating ligands, aggregation (aggregation-induced emission mechanism) [129,131–133], doping with silver such as in rod-shaped $[Au_{25-x}Ag_x(PPh_3)_{10}(SC_2H_4Ph)_5Cl_2]^{2+}$ (QY = 40–60%) [134]. Or rigidification of the shell [131,135].

12.5. Chiral Nanoclusters

The origins of chirality of nanoclusters are either due to the core, to the ligands or to both [136,137]. For instance, the Au_{18} kernel of $Au_{25}(SR)_{18}$ has an inversion center and symmetry plane, therefore the cluster is achiral, which shows that the chirality of $Au_{25}(SR)_{18}$ clusters is due to ligands [55]. Chiral enantiomers were first isolated by Bürgi upon HPLC isolation [138]. In the cluster $Au_{133}(SR)_{52}$, it was shown that chirality was not due to the kernel that was achiral, but to the arrangements of interfacial -S-Au-S- ladder-like helical "stripes" and further to the "swirls" of carbon tails, because the direction of rotations of the swirls, each composed of four Ph-^{t}Bu tails, is different in the two enantiomers. [139]. The inner Au_5 core of Au_{13} contributes to chirality via transition state density and torsion analysis determined by DFT, as shown by Shichibu et al. [140]. Thus, while the chiral ligands have a dominant effect in the CD activity, Au_{13} itself has an intrinsic metal core chirality.

12.6. Catalysis

Catalysis by nanogold has long been known, especially since Haruta's group discovered in 1987 that oxide-supported small AuNPs ≈5 nm were very active in CO oxidation even at −70 °C [141]. In addition, another remarkable result by Haruta was the discovery of the direct synthesis of hydrogen peroxide (H_2O_2) from O_2 and H_2 over AuNPs supported on TiO_2 [142]. Given the inactivity of bulk gold metal, these seminal findings dramatically marked the beginning of catalysis by small gold AuNPs and Au NCs. Considerable studies have then

been devoted to AuNPs on catalysis of selective oxidation, hydrogenation, cross coupling reactions, and CO_2 conversion [143–150].

Subsequently, the various Au NCs with ligands have been investigated in catalysis [55,78,141–153]. In general, Au phosphine clusters are good catalysts, because phosphine ligands are easily removed thermally from the Au core surface, for instance upon heating to 200 °C, but then the Au NCs are transformed into AuNPs in the catalytic process, even when the catalysis is conducted at lower temperature such as 80 °C to 100 °C [106]. Many works have been reported with Au-phosphine clusters as catalysts for oxidation, hydrogenation and photocatalysis reactions [106]. Au clusters such as glutathione-Au_x clusters are narrow bandgap photosensitizers, like semiconductors, and co-catalysts, which have shown use, for instance on Au/TiO_2, for water splitting, photodegradation of dyes and photoreduction of aromatic nitro compounds [121]. The challenge in Au NC catalysis is to establish a relationship between the Au NC structure and the catalytic activity. A first step is to find clusters that keep catalytic activity without structural change. For instance, the catalyst $Au_{11}(PPh_3)_7Cl_3/SiO_2$ was found to be robust enough, as it showed no decrease in activity after six catalytic cycles [122].

The three gold nanoclusters $[Au_9(PPh_3)_8](NO_3)_3$ (in short Au_9), $[Au_{11}(PPh_3)_8Cl_2]Cl$ (in short Au_{11}), and $Au_{36}(TBBT)_{24}$ (in short Au_{36}; TBBT = 4-*tert*-butylbenzenethiol) were shown to catalyze in distinctly different ways CO_2 hydrogenation. The Au_9, Au_{11}, and Au_{36}, catalysts selectively yielded methane, ethane and formic acid, respectively (selectivities between 80 and 90%). These selectivity differences were taken into account, using DFT calculations, by the relative binding strengths of the Au surface with the H* adatom and *CO crucial intermediates that were all the weaker as the Au nuclearity increased [154] (Figure 22).

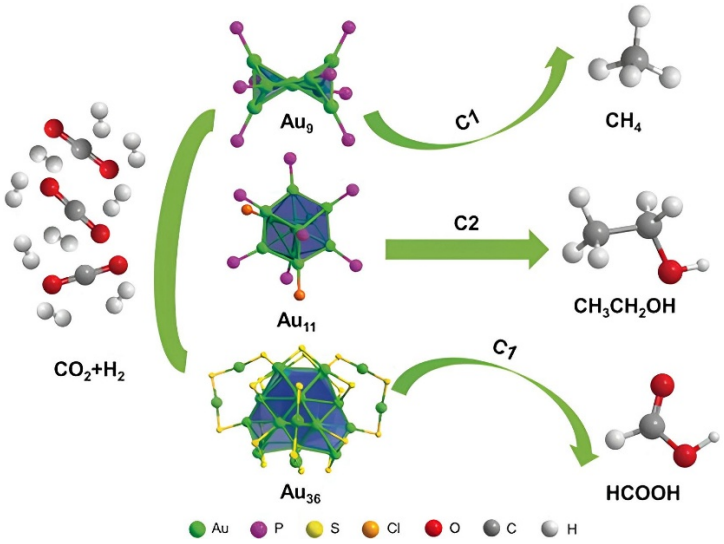

Figure 22. Compared catalytic activities of the three gold nanoclusters $[Au_9(PPh_3)_8](NO_3)_3$ (in short Au_9), $[Au_{11}(PPh_3)_8Cl_2]Cl$ (in short Au_{11}), and $Au_{36}(TBBT)_{24}$ (in short Au_{36}; TBBT = 4-tert-butylbenzenethiol) in CO_2 hydrogenation reactions taken into account by the relative binding strengths of the Au surface with the H* adatom and *CO crucial intermediates that were all the weaker as the Au nuclearity increased. Reprinted with permission from ref. [154] (groups of Y. Zhu' and Zhou). Copyright Wiley-VCH 2020.

Many studies have focused on the $Au_{25}(SR)_{18}$ nanoclusters, as illustrated by the few examples below. Without any activation treatment (e.g., ligand removal), the ceria-supported $Au_n(SR)_m/CeO_2$ catalyst was found to exhibit CO oxidation activity at an onset temperature of 60 °C [155]. Jin's group explored the $Au_{25}(SR)_{18}$ nanocluster (supported on oxides) for the semihydrogenation of alkynes to alkenes using H_2 as the hydrogen source [156], the Sonogashira cross-coupling reaction using a CeO_2-supported $Au_{25}(SR)_{18}$ (R = CH_2CH_2Ph) nanocluster catalyst [157] and catalysis by supported $[Au_{25}(SR)_{18}]^-$ for the electrocatalytic reduction of CO_2 [158]. This CO2RR reaction presently is one of the most intensively studied for an energetic purpose. For instance, a recent comparison of thiolate Au-25, Au-38, and Au-144 nanoclusters as model catalysts showed that remarkably high CO2RR activity was obtained, increasing with increasing the Au NC size. Dethiolated Au sites were the active sites and the CO2R catalytic activity depended on the number of active sites on the gold surface [159]. *N*-heterocyclic carbene (NHC)-Au clusters, synthesized by ligand exchange using $Au_{11}(PPh_3)_3Cl_3$ as precursor also exhibited good catalytic performance in CO_2RR, with over 80% Faraday efficiency for CO, together with high current density and mass activity [160]. The field of CO2RR catalyzed by gold APNC has recently been reviewed by Zhao, Ziarati and Bürgi [161].

12.7. Photocatalysis

Plasmon irradiation of AuNPs (visible region) is well-known not only to bring about their beautiful colors [1,11,15], but also to excite electron in nearby Au-catalyst bonds boosting the catalytic activity of other nanomaterials [162–165]. This was shown for instance for hydrogen (H_2) production in Au-metal catalyzed ammonia borane hydrolysis [164–166]. The situation is different in gold APNCs with sizes below 2.3 nm, because they do not present a plasmon band, but molecule-like discrete molecular orbital levels. Light irradiation of the photocatalyst then provokes photon absorption that excite electrons, forming electron pairs between electrons and electron holes, which are well separated due to the discrete energy levels. The optical absorption essentially arises from intra-valence band HOMO–LUMO transitions. In this way, the large surface of metal clusters provokes a high density of active sites, facilitating reactions. In addition, integrating metal clusters with other semiconductors forms heterojunctions that favor charge separation and further photostability and photocatalysis. Defect engineering uses mid-gap states for stabilization of the photocatalyst, favoring photoactivity in the visible region. Doping, for instance, Au clusters with Ag introduces synergy and improves photocatalytic performances. Increased photocatalytic activity can also be obtained upon introduction in the cluster a of metal ion, metal atom or another nanomaterial for solar-powered photoredox catalysis systems including organic pollutant mineralization, selective organic transformation, hydrogen generation, CO_2 reduction, and water splitting [167].

Photocatalytic properties of $Au_{25}(SG)_{18}$ nanoclusters were reported and Tatsuma' group with Au_{25}-modified TiO_2 under visible and near infrared light [168] and with glutathione-protected gold clusters adsorbed on TiO_2 electrodes [169], and the area of photocatalysis by APNCs [170] and alloys [171] (including gold) has recently been reviewed by several groups [168–170], with special attention to CO_2 photocatalytic activation [40].

12.8. Biomedical Applications

The biological applications of gold NPs are well-known and have been (and still are) widely exploited [14–29,172]. Concerning gold subnanoclusters, they are photostable and highly fluorescent, in particular $Au_{18}(SG)_{25}$ that is water soluble. Thus, they hold great promise as ultrabright biolabels and light-emitting sources. They can be readily conjugated with a variety of biological molecules, with applications in fluorescent biological imaging and therapeutically oriented detection [173–179]. For instance, Pradeep and co-workers demonstrated the use of luminescent Au_{23} for Cu^{2+} sensing [173] and the Xie group demonstrated the potential of $Au_n(SG)_m$ clusters as radiosensitizers for cancer radiotherapy [179]. Generally, nanoclusters can also be designed, with recent applications reported as antibacterial, drug delivery and cancer therapy systems [180]. The introduction of tetraethyleneglycol chains on NHC ligands of $[Au_{13}(NHC)_5Br_2]Br_3$ allowed solubilization in water for in vivo toxicity studies [181]. The intrinsic toxicity of among other nanomaterials has been evaluated to be minimum [182], and that of nanoclusters depends on their size as illustrated by Simon's work [183].

13. Recent Trends

Research on gold and other APNCs is currently continuing, with intense activity in the fundamental and applied fields. The recent trends are in the elaboration of more complex APNC frameworks including composite nanomaterials and their applications in biosensing, therapy, imaging and various catalytic aspects including in particular photocatalysis and electrocatalysis.

13.1. Super-Structures

Nanocluster superstructures have been constructed through ordered self-assembly aggregation yielding hierarchical nanomaterals resulting from driving forces involving ligand-ligand, metal-ligand, and metal-metal interactions, as well as interactions with other compounds [184]. Such self-assembled gold and silver nanoclusters allow the fabrication of films, 2D nanosheets, colloidal crystals and macroscopic membranes with specific properties and applications [185]. Ligand engineering is crucial for the design of APNCs with targeted applications and mostly involves ligand exchange strategies that have been recently reviewed [186]. For instance, ligand exchanges can be designed for the introduction of polyoxometallates that stabilize the gold APNCs. Such assemblies exhibit synergistic and cooperative interactions enabling the emergence of new properties [187]. Another noteworthy unit that can be introduced into APNCs upon ligand exchange is carborane that has a spherical shape and three-dimensional aromaticity, providing electronic effects. The incorporation of carborane into ligands has allowed the construction of nanoclusters exhibiting distinct architectures, enhanced stability, and unique reactivity [188]. Subtle intra and inter-cluster non-covalent interactions such those between two H-bonded atoms or between C-H bonds and aromatic rings can provoke the self-assembly of some APNCs into various

superstructures with compact helical conformations comparable to folded states in natural proteins. Such helical assemblies were shown to amplify specifically triggered physicochemical properties with potential applications in chiral recognition, enantioselective catalysis, molecular sensing and photoluminescence [189]. The remarkable photophysical properties of mono- and dinuclear alkynyl-gold and other supramolecular complexes could even find synergistic enhancement with gold APNCs [190].

13.2. Biomedical Applications

APNCs are promising for cancer imaging and treatment, due to their excellent cancer-targeting capabilities, high imaging signal-to-noise ratio, potential anti-cancer activity, efficiency for in vivo clearance, and biocompatibility. This field of essential applicative research has very recently been reviewed [191–193]. For instance, gold nanoclusters have been utilized combined with nanobubbles, that have potential to reverse tumor hypoxia, to detect and eradicate residual cancer cells after surgery, while being site-specific and minimally invasive [194]. The fluorescence of gold and other nanoclusters continues to attract attention in relation with biological applications toward bioimaging and biosensing [195,196], as for instance with antibacterials [197,198] or for monitoring apoptosis [199].

13.3. Catalysis

Nanocluster catalysis has become a very active subfield of catalysis. Of particular interest is the relationship between the nanocluster structure and its catalytic properties [153]. The methods allowing to engineer gold nanocluster catalytic activity have been shown to include post-treatment, the bulky ligands strategy, the surface geometric mismatch method, and doping by another crucial metal or herteroatom [200,201]. Ligand engineering in APNC catalysis is a crucial aspect, including the use of a ligand library [202]. Another strategy has recently involved hybridizing APNCs with various components to synthesize APNC-based hybrid nanomaterials in order to obtain stabilizing and synergistic effects [203,204]. Although purely gold-cored clusters are effective catalysts that can be tuned [205,206], it is now clear that heterobimetallic gold clusters benefit from superior performances due to the synergy between atoms of different natures, and this has recently been shown to be especially true for energy related catalytic transformation of small molecules [207]. Among the gold or alloyed APNC-catalyzed reactions, the most frequently examined have recently been the photocatalytic [170,171] and electrocatalytic [204–208] CO_2 reduction reactions. New experimental beam techniques, together with mass spectrometry and laser spectroscopy, improve the investigations of electronic, optical, magnetic, catalytic properties of isolated clusters as a function of their sizes [209].

14. Conclusions

Following the considerable usage of gold nanoparticles for milleniums and two centuries of scientific scrutiny, their applications have spread in the three last decades due to their remarkable stabilization since the 1990's by thiolate ligands. Thiolated AuNPs have been applied in cancer theranostic, most often using their plasmon bands for phototherapy and sensing, but also for many anti-cancer drug deliveries (taxanes, etc.) [210]. The combination of gold nanoparticles with a variety of molecules [211] and materials [212] also makes them excellent sensors, drug delivery therapeutics [213] and catalysts [214,215].

In parallel, Au APNCs have been synthesized with carbonyl (bimetallic) and phosphine ligands since the 1980's, in particular the Au_{13} clusters, such as the first 8-electron icosahedral cluster $[Au_{13}(PPhMe_2)_{10}Cl_2]$ $(PF_6)_3$, predicted, then synthesized by Mingos' group. With thiolate ligands, one of the key differences between AuNPs and Au APNCs is that AuNPs are easily synthesized from $HAuCl_4$ directly using $NaBH_4$ or a large variety of other reducing agents, whereas, on the contrary, the direct use of $HAuCl_4$ with a variety of reductants led to complex mixtures of thiolate Au APNCs, until the selective synthesis of Au APNCs was shown by Jin's group to be best conducted by reduction of Au(I) species. The two more recent families of aryl APNCs and carbene APNC revealed in the 2010's brought about new rich fundamental and applied aspects, given their stabilities together with electronic, sensing ad catalytic properties. For example, theoretical studies have shown that the icosahedral core can isomerize to slightly less compact cuboctahedral core depending of the NHC carbene ligand shape and size in NHC-gold clusters [216], which might impact catalytic properties. The latter could also be modulated by ligand library, a concept applicable to a variety of metal clusters and alloys [217].

The photophysical properties of several families of gold APNCs have shown excellent bioimaging and biosensing applications, and their drug delivery functions will continue their promising development in the future. The research of new gold and alloyed APNC and derived nanomaterials shows infinite structural possibilities that will excite the creativity of researchers and will provide improved applications in biomedicine, materials science

and catalysis, following Haruta's pioneering discoveries in the 1980's. Given these recent trends and conclusions, it can safely be anticipated that the fields of AuNPs, Au APNCs and their derived hybrid nanomaterials will have a bright future.

Note Added in Proofs

Recently, near-unity NIR phosphorescent quantum yield was observed for a $Au_{16}Cu_6$ nanocluster [218], asymmetric catalytic applications of chiral APNCs have been reviewed [219], and the electrical properties of Au_{25} APNCs have been tuned through metal-ion-mediated assembly [220].

Author Contributions

Credit: H.W.: methodology, investigation, software, data curation, visualization; J.-L.P.: supervision, validation; D.A.: writing—reviewing and editing. All authors have read and agreed to the published version of the manuscript.

Funding

This research received no external funding.

Data Availability Statement

Accessibility of data in this review is accessible by the authors upon reasonable request.

Acknowledgments

We warmly thank the Executive Editor-in-Chief, the Reviewers and Jean-René Hamon (Univ. Rennes) for helpful comments and the co-authors cited in the references for their excellent contributions to the ideas and work accomplishments. Financial support from the Chinese Scholarship Council (CSC grant to HW), the University of Bordeaux and the Centre National de la Recherche Scientifique (CNRS) is gratefully acknowledged.

Conflicts of Interest

Given his role in the journal, Editor-in-Chief, Didier Astruc had no involvement in the peer review of this paper and had no access to information regarding its peer-review process. Full responsibility for the editorial process of this paper was delegated to another editor of the journal. The authors take full responsibility for the content of the published article.

Use of AI and AI-Assisted Technologies

No AI tools were utilized for this paper.

Abbreviations

AFM	atomic force microscopy
APNC	atomically precise nanocluster
AuNP	gold nanoparticle
CD	circular dichroism
DFT	Density functional theory
DNA	desoxyribonucleic acid
EPTH	ethynyl-phenanthrene
ESI-MS	electrospray ionization-mass spectrometry
EXAFS	Extended X-Ray Absorption Fine Structure
Fc	ferrocenyl
Hdpa	2,2′-dipyridylamine
HOMO	highest occupied molecular orbital
LRSSPP	Long Range Surface Plasmon Polariton

LSPR	Localized Surface Plasmon Resonance
LUMO	Lowest Unoccupied Molecular Orbital
MALDI-MS	Matrix-assisted laser desorption/ionization mass spectrometry
NHC	N-Heterocyclic Carbene
NC	nanocluster
NP	nanoparticle
PAH	phenylacetylene
p-MBA	*p*-mercaptobenzoic acid
PVP	polyvinylpyrrolidone
RNA	Ribonucleic acid
SERS	Surface Enhanced Raman Scattering
SGH	glutathione
SPR	Surface Plasmon Resonance
TBBT	4-tert-butylbenzenethiol
TEM	transmission electron microscopy
TOAB	tetraoctylammonium bromide

References

1. Daniel, M.C.; Astruc, D. Gold Nanoparticles: Assembly, Supramolecular Chemistry, Quantum-Size-Related Properties, and Applications toward Biology, Catalysis, and Nanotechnology. *Chem. Rev*. **2004**, *104*, 293–346.
2. Antonii, F. *Panacea Aurea-Auro Potabile*; Bibliopolio Frobeniano: Hamburg, Germany, 1618.
3. Kahn, R.L. Serum Diagnosis for Syphilis. *Colloid Chem*. **1928**, *2*, 757.
4. Faraday, M. Experimental Relations of Gold (and other Metals) to Light. *Philos. Trans.* **1857**, *147*, 145–181.
5. Mie, G. Beiträge zur optik trüber medien, speziell kolloidaler metallösungen. *Ann. Phys.* **1908**, *330*, 377–445.
6. Schmid, G. Large Clusters and Colloids. *Chem. Rev*. **1992**, *92*, 1709–1727.
7. Jin, R.C.; Zeng, C.J.; Zhou, M.; Chen, Y.X. Atomically Precise Colloidal Metal Nanoclusters and Nanoparticles: Fundamentals and Opportunities. *Chem. Rev*. **2016**, *116*, 10346–10413.
8. Li, S.; Li, N.N.; Mak, T.C.W. Chemical Flexibility of Atomically Precise Metal Clusters. *Chem. Rev*. **2024**, *124*, 7262–7378.
9. Chakraborty, I.; Pradeep, T. Atomically Precise Clusters of Noble Metals: Emerging Link between Atoms and Nanoparticles. *Chem. Rev*. **2017**, *117*, 8208–8271.
10. Chen, S.; Ingram, R.S.; Hostetler, M.J.; Pietron, J.J.; Murray, R.W.; Schaaff, T.G.; Whetten, R.L. Gold Nanoelectrodes of Varied Size: Transition to Molecule-Like Charging. *Science* **1998**, *280*, 2098–2101.
11. Quinn, B.M.; Liljeroth, P.; Ruiz, V.; Laaksonen, T.; Kontturi, K. Electrochemical Resolution of 15 Oxidation States for Monolayer Protected Gold Nanoparticles. *J. Am. Chem. Soc.* **2003**, *125*, 6644–6645.
12. Myroshnychenko, V.; Rodríguez-Fernández, J.; Pastoriza-Santos, I.; Funston, A.M.; Novo, C.; Mulvaney, P.; De Abajo, F.J.G. Modelling the optical response of gold nanoparticles. Modelling the optical response of gold nanoparticles. *Chem. Soc. Rev*. **2008**, *37*, 1792–1805.
13. Sun, Y.G.; Xia, Y.G. Shape-controlled Synthesis of Gold and Silver Nanoparticles. *Science* **2002**, *298*, 2176–2179.
14. Anker, J.N.; Hall, W.P.; Lyandres, O.; Shah, N.C.; Zhao, J.; Van Duyne, R.P. Biosensing with Plasmonic Nanosensors. *Nat. Mater*. **2008**, *7*, 442–453.
15. Boisselier, E.; Astruc, D. Gold Nanoparticles in Nanomedicine: Preparations, Imaging, Diagnostics, Therapies and Toxicity. *Chem. Soc. Rev*. **2009**, *38*, 1759–1782.
16. Mirkin, C.A.; Letsinger, R.L.; Mucic, R.C.; Storhoff, J.J. A DNA-based Method for Rationally Assembling Nanoparticles into Macroscopic Materials. *Nature* **1996**, *382*, 607–609.
17. Huang, X.; El-Sayed, I.H.; Qian, W.; El-Sayed, M.A. Cancer Cell Imaging and Photothermal Therapy in the Near-infrared Region by Using Gold Nanorods. *J. Am. Chem. Soc.* **2006**, *128*, 2115–2120.
18. Llevot, A. D. Astruc. Applications of Vectorized Gold Nanoparticles to the Diagnosis and Therapy of Cancer. *Chem. Soc. Rev*. **2012**, *41*, 242–257.

19. Patra, J.K.; Das, G.; Fraceto, L.F.; Campos, E.V.R.; Rodriguez-Torres, M.D.P.; Acosta-Torres, L.S.; Shin, H.S. Nano Based Drug Delivery Systems: Recent Developments and Future Prospects. *J. Nanobiotechnol*. **2018**, *16*, 71.
20. Kastner, S.; Dietel, A.K.; Seier, F.; Ghosh, S.; Weiß; D; Makarewicz, O.; Fritzsche, W. LSPR-based Biosensing Enables the Detection of Antimicrobial Resistance Genes. *Small* **2023**, *19*, e2207953.
21. Gu, R.; Duan, Y.; Li, Y.; Luo, Z. Fiber-optic-based Biosensor as an Innovative Technology for Point-of-care Testing Detection of Foodborne Pathogenic Bacteria to Defend Food and Agricultural Product Safety. *J. Agric. Food Chem*. **2023**, *71*, 10982–10988.
22. Qu, J.H.; Dillen, A.; Saeys, W.; Lammertyn, J.; Spasic, D. Advancements in SPR Biosensing Technology: An Overview of Recent Trends in Smart Layers Design, Multiplexing Concepts, Continuous Monitoring and in vivo Sensing. *Anal. Chim*. *Acta.* **2020**, *1104*, 10–27.
23. Ravindran, N.; Kumar, S.; Yashini, M.; Rajeshwari, S.; Mamathi, C.A.; Nirmal, T.S.; Sunil, C.K. Recent advances in surface plasmon resonance (SPR) biosensors for food analysis: A review. Crit. Rev. *Food Sci. Nutr*. **2023**, *63*, 1055–1077.
24. Itoh, T.; Procházka, M.; Dong, Z.-C.; Ji, W.; Yamamoto, Y.S.; Zhang, Y.; Osaki, Y. Toward a new era of SERS and TERS at the nanometer scale: From fundamentals to innovative applications. *Chem. Rev*. **2023**, *123*, 1552–1634.
25. Lin, H.C.; Lee, Y.; Lin, C.C.; Ho, Y.-L.; Xing, D.; Chen, M.-H.; Lin, B.-W.; Chen, L.-Y.; Chen, C.-W.; Delaunay, J.-J. Integration of on-chip perovskite nanocrystal laser and long-range surface plasmon polariton waveguide with etching-free process. *Nanoscale* **2022**, *14*, 10075–10081.
26. Yang, L.; Wang, J.; Altreuter, J.; NJhaveri, A.; Wong, C.J.; Song, L.; Fu, J.; Taing, L.; Bodapati, S.; Sahu, A.; Tkheim, C.; Zhang, Y.; Zeng, Z.; Bai, G.; Tang, M.; Qiu, X.; Long, H.W.; Michor, F.; Liu, Y.; Liu, X.S. Tutorial: Integrative computational analysis of bulk RNA-sequencing data to characterize tumor immunity using RIMA. *Nat. Protoc.* **2023**, *18*, 2404–2414.
27. Lu, F.; Astruc, D. Nanomaterials for Removal of Toxic Elements from Water. *Coord. Chem. Rev.* **2018**, *356*, 47–164.
28. Nanda, B.P.; Rani, P.; Paul, P.; Aman; Ganti, S.S.; Bhatia, R. Recent Trends and Impact of Localized Surface Plasmon Resonance (LSPR) and Surface-enhanced Raman Spectroscopy (SERS) in Modern Analysis. *J. Pharmaceut. Anal*. **2024**, *14*, 100959.
29. Saha, K.; Agasti, S.S.; Kim, C.; Li, X.N.; Rotello, V.M. Gold Nanoparticles in Chemical and Biological Sensing. *Chem. Rev*. **2012**, *112*, 2739–2779.
30. Turkevitch, J.; Stevenson, P.C.; Hillier, J. A Study of the Nucleation and Growth Process in the Synthesis of Colloidal Gold Discuss. *Faraday Soc.* **1951**, *11*, 55–75.
31. Frens, G. Controlled Nucleation for the Regulation of the Particle Size in Monodisperse Gold Suspensions. *Nature: Phys. Sci.* **1973**, *241*, 20–22.
32. Yonezawa, T.; Kunitake, P. Practical Preparation of Anionic Mercapto Ligand-Stabilized Gold Nanoparticles and Their Immobilization. *Colloids Surf. A Physicochem. Eng. Asp*. **1999**, *149*, 193–199.
33. Zhao, P.X.; Li, N.; Astruc, D. State of the art in gold nanoparticle synthesis. *Coord. Chem. Rev.* **2013**, *257*, 638–665.
34. Giersig, M.; Mulvaney, P. Preparation of Ordered Colloid Monolayers by Electrophoretic Deposition. *Langmuir* **1993**, *9*, 3408–3413.
35. MBrust; Walker, M.; Bethell, D.; Schiffrin, D.J.; Whyman, R.J. Synthesis of Thiol-Derivatized Gold Nanoparticles in a Two-phase Liquid–Liquid System. *J. Chem. Soc. Chem. Commun.* **1994**, *7,* 801–802.
36. BPrasad, L.V.; Stoeva, S.I.; Sorensen, C.M.; Klabunde, K.J. Digestive-Ripening Agents for Gold Nanoparticles: Alternatives to Thiols. *Chem. Mater.* **2003**, *15*, 935–942.
37. Andres, R.P.; Bielefeld, J.D.; Henderson, J.I.; Janes, D.B.; Kolagunta, V.R.; Kubiak, C.P.; Mahoney, W.J.; Ogifsin, R.G. Self-Assembly of a Two-Dimensional Superlattice of Molecularly Linked Metal Clusters. *Science* **1996**, *273*, 1690–1693.
38. Brust, M.; Fink, J.; Bethell, D.; Schiffrin, D.J.; Kiely, C.J. Synthesis and Reactions of Functionalised Gold Nanoparticles. *J. Chem. Soc. Chem. Commun*. **1995**, 1655–1656.
39. Hostetler, M.J.; Templeton, A.C.; Murray, R.W. Dynamics of Place-Exchange Reactions on Monolayer-Protected Gold Cluster Molecules. *Langmuir* **1999**, *15*, 3782–3789.
40. Liu, M.Y.; Guo, R.-T.; Liu, C.; Cui, H.F.; Zhu, H.W.; Pan, W.G. Research progress in photocatalytic reduction of CO_2 based on metal nanocluster materials. *J. Mater. Chem. A* **2024**, *12*, 32665–32688.
41. Xia, Y.N.; Xiong, Y.J.; Skrabalak, S.E. Shape-controlled Synthesis of Metal Nanocrystals: Simple Chemistry Meets Complex Physics. *Angew. Chem. Int. Ed*. **2009**, *48*, 60–103.
42. Li, N.; Zhao, P.; Astruc, D. Anisotropic gold nanoparticles: Synthesis, properties, applications, and toxicity. *Angew. Chem. Int. Ed.* **2014**, *53*, 1756–1789.
43. Nikoobakht, B.; El-Sayed, M.A. Preparation and Growth Mechanism of Gold Nanorods (NRs) Using Seed-Mediated Growth Method. *Chem. Mater*. **2013**, *15*, 1957–1962.

44. Shiratori, K.; West, C.A.; Jia, Z.; Lee, S.A.; Cook, E.A.; Murphy, C.J.; Landes, C.F.; Link, S. Machine Learning to Adaptively Predict Gold Nanorod Sizes on Different Substrates. *J. Phys. Chem. C* **2025**, *129*, 5913–5920.
45. Jin, R.; Qian, H.; Wu, Z.; Zhu, Y.; Zhu, M.; Mohanty, A.; Garg, N. Size Focusing: A Methodology for Synthesizing Atomically Precise Gold Nanoclusters, *J. Phys. Chem. Lett.* **2010**, *1*, 2903–2910.
46. Cotton, F.A. Transition-metal Compounds Containing Clusters of Metal Atoms. *Q. Rev. Chem. Soc.* **1966**, *20*, 389–401.
47. Astruc, D. Electron-Transfer Chain Catalysis in Organo-Transition-Metal Chemistry. *Angew. Chem., Int. Ed. Engl.* **1988**, *27*, 643–660.
48. Alonso, E.; Astruc, D. Introduction of the Cluster Fragment $Ru_3(CO)_{11}$ at the Periphery of Phosphine Dendrimers Catalyzed by the Electron-Reservoir Complex $[Fe^{I}Cp(C_6Me_6)]$. *J. Am. Chem. Soc*. **2000**, *122*, 3222–3223.
49. Goswani, N.; Yao, Q.; Chen, T.; Xie, J. Mechanistic Exploration and Controlled Synthesis of Precise Thiolate-gold Nanoclusters. *Coord. Chem. Rev.* **2016**, *329*, 1–15.
50. Negishi, Y.; Nobusada, K.; Tsukuda, T. Glutathione-protected Gold Clusters Revisited: Bridging the Gap Between Gold(I)-thiolate Complexes and Thiolate-Protected Gold Nanocrystals. *J. Am. Chem. Soc*. **2005**, *127*, 5261–5270.
51. Wu, Z.; MacDonald, M.A.; Chen, J.; Zhang, P. Jin. Kinetic Control and Thermodynamic Selection in the Synthesis of Atomically Precise Gold Nanoclusters. *J. Am. Chem. Soc.* **2011**, *133*, 9670–9673.
52. Kang, X.; Chong, H.B.; Zhu, M.Z. $Au_{25}(SR)_{18}$: The Captain of the Great Nanocluster Ship. *Nanoscale* **2018**, *10*, 10758–10834.
53. Zhu, M.; Lanni, E.; Garg, N.; Bier, M.E.; Jin, R. High-Yield Synthesis of Au_{25} Clusters, *J. Am. Chem. Soc*. **2008**, *130*, 1138.
54. Zhu, M.; Aikens, C.M.; Hollander, F.J.; Schatz, G.C.; Jin, R. Correlating the Crystal Structure of a Thiol-Protected Au_{25} Cluster and Optical Properties. *J. Am. Chem. Soc.* **2008**, *130*, 5883–5885.
55. Pan, P.Y.; Kang, X.; Zhu, M.Z. Preparation Methods of Metal Nanoclusters. *Chem. Eur. J.* **2025**, *31*, e202404528.
56. Qian, H.; Zhu, Y.; Jin, R. Optical and Electrochemical Properties of Monodisperse $Au_{38}(SC_2H_4Ph)_{24}$ Nanoclusters. *ACS Nano* **2009**, *3*, 3795–3803.
57. Qian, H.; Eckenhoff, W.T.; Zhu, Y.; Pintauer, T.; Jin, R. Total Structure Determination of Thiolate-Protected Au_{38} Nanoparticles. *J. Am. Chem. Soc*. **2010**, *132*, 8280–8281.
58. Yan, J.Z.; Teo, B.K.; Zheng, N.F. Surface Chemistry of Atomically Precise Coinage-Metal Nanoclusters: From Structural Control to Surface Reactivity and Catalysis. *Acc. Chem. Res.* **2018**, *51*, 3084–3093.
59. Matus, M.F.; Häkkinen, H. Understanding Ligand-protected Noble Metal Nanoclusters at Work. *Nat. Rev. Mater*. **2023**, *8*, 372–389.
60. Yao, Q.F.; Zhu, M.S.Q.; Yang, Z.C.; Song, X.R.; Yuan, X.; Zhang, Z.P.; Hu, W.P.; Xie, J.P. Molecule-like synthesis of ligand-protected metal nanoclusters. *Nat*. *Rev*. *Mater.* **2024**, *10*, 89–108.
61. Lyu, J.K.; Qian, J.; Yang, Z.C.; Xie, J.P. Synthesis planning for atomically precise metal nanoclusters. *Nanoscale Horiz.* **2025**, *10*, 2304–2339.
62. Jin, S.; Wang, S.; Zhu, M.Z. Clusters and their alloys based on M_{13} units. *Chem. Asian J.* **2025**, *14*, 3222–3231.
63. Wade, K. Structural Significance of number of skeletal bonding electron-pairs in carboranes, higher boranes and borane anions, and various transition-metal carbonyl cluster Compounds. *J. Chem. Soc. Chem. Commun*. **1971**, *15*, 792–793.
64. Astruc, D. *Organometallic Chemistry and Catalysis*; Springer: Berlin, Germany, 2007; Chapter 2, pp. 47–76. https://doi.org/10.1007/978-3-540-46129-6.
65. Chini, P. Large metal carbonyl clusters (LMCC). *J. Organomet. Chem*. **1980**, *200*, 37–61.
66. Walter, M.; Akola, J.; Lopez-Acevedo, O.; Jadzinsky, P.D.; Calero, G.; Ackerson, C.J.; Whetten, R.L.; Grönbeck, H.; Häkkinen, H. A unified view of ligand-protected gold clusters as superatom complexes. *Proc. Natl. Acad. Sci. USA* **2008**, *105*, 9157–9162.
67. I. Katakuse, T. Hichihara, Y. Fujita, T. Matsuo, T. Sakurai, H. Matsuda, Mass distributions of copper, silver and gold clusters and electronic shell structure. *Intern. J. Mass Spectrom. Ion Process.* **1985**, *67*, 229–236.
68. Mingos, D.M.P. Molecular-orbital calculations on cluster compounds of gold. *J. Chem.* Soc. *Dalton Trans.* **1976**, *13*, 1163.
69. Briant, C.E.; Theobald, B.R.C.; White, J.W.; Bell, L.K.; Mingos, D.M.P. Synthesis and X-ray crystal structure of the centred icosahedral gold cluster compound $[Au_{13}(PPhMe_2)_{10}Cl_2]$ $(PF_6)_3$, the realization of a theoretical prediction. *J. Chem. Soc. Chem. Commun.* **1981**, *5*, 201–202.
70. He, W.M.; Hu, H.; Cui, Y.J.; Li, J.; Si, Y.B.; Wang, S.B.; Zhao, Y.J.; Zhou, Z.; Ma, L.F.; Zang, S.-Q. Filling the gaps in icosahedral superatomic metal clusters. *Nat. Sci. Rev*. **2024**, *11*, 174.
71. Heaven, W.; Dass, A.; White, P.S.; Holt, K.M.; Murray, R.W. Crystal structure of the gold nanoparticle $[N(C_8H_{17})_4][Au_{25}(SCH_2CH_2Ph)_{18}]$. *J. Am. Chem. Soc.* **2008**, *130*, 1354–1355.
72. Lavenn, C.; Albrieux, F.; Bergeret, G.; Chiriac, R.; Delichère, P.; Tuel, A. Functionalized gold magic clusters: $Au_{25}(SPhNH_2)_{17}$. *Nanoscale* **2012**, *4*, 7334–7337.

73. Akola, J.; Walter, M.; Whetten, R.; Häkkinen, H.; Grönbeck, H. On the Structure of Thiolate-Protected Au_{25}. *J. Am. Chem. Soc.* **2008**, *130*, 3756–3757.
74. Mackay, A.L. A dense non-crystallographic packing of equal spheres. *Acta Crystallogr.* **1962**, *15*, 916–918.
75. Jadzinsky, P.D.; Calero, G.; Ackerson, C.J.; Bushnell, D.A.; Kornberg, R.D. Structure of a Thiol Monolayer-Protected Gold Nanoparticle at 1.1 Å Resolution. *Science* **2007**, *318*, 430–433.
76. Yao, Q.; Yuan, X.; Fung, V.; Yu, Y.; Leong, D.T.; Jiang, D.-E.; Xie, J. Understanding seed-mediated growth of gold nanoclusters at molecular level. *Nat. Commun.* **2017**, *8*, 927.
77. Xiao, Q.; Chen, T.; Yuan, X.; Xie, J. Toward Total Synthesis of Thiolate-Protected Metal Nanoclusters. *Acc. Chem. Res*. **2018**, *51*, 1338–1348.
78. Kang, X.; Li, Y.; Zhu, M.Z.; Jin, R.C. Atomically precise alloy nanoclusters: Syntheses, structures, and properties. *Chem. Soc. Rev.* **2020**, *49*, 6443–6514.
79. Maity, P.; Tsunoyama, H.; Yamauchi, M.; Xie, S.H.; Tsukuda, T. Organogold Clusters Protected by Phenylacetylene, *J. Am. Chem. Soc.* **2011**, *133*, 20123–20125.
80. Maity, P.; Wakabayashi, T.; Ichikuni, N.; Tsunoyama, H.; Xie, S.; Yamauchi, M.; Tsukuda, T. Selective synthesis of organogold magic clusters $Au_{54}(C{\equiv}CPh)_{26}$. *Chem. Commun.* **2012**, *48*, 6085–6087.
81. Maity, P.; Takano, S.; Yamazoe, S.; Wakabayashi, T.; Tsukuda, T. Binding Motif of Terminal Alkynes on Gold Clusters. *J. Am. Chem. Soc.* **2013**, *135*, 9450–9457.
82. Wan, X.-K.; Guan, Z.-J.; Wang, Q.-M. Homoleptic Alkynyl-Protected Gold Nanoclusters: $Au_{44}(PhC{\equiv}C)_{28}$ and $Au_{36}(PhC{\equiv}C)_{24}$. *Angew. Chem. Int. Ed.* **2017**, *56*, 11494–11497.
83. Lei, Z.; Li, J.-J.; Wan, X.K.; Wang, Q.M. Isolation and Total Structure Determination of an All-Alkynyl-Protected Gold Nanocluster Au_{144}. *Angew. Chem. Int. Ed.* **2018**, *57*, 8639–8643.
84. Lei, Z.; Wan, X.K.; Yuan, S.F.; Wang, J.Q.; Wang, Q.M. Alkynyl-protected gold and gold–silver nanoclusters. *Dalton Trans*. **2017**, *46*, 3427–3434.
85. Wang, Y.; Su, H.; Xu, C.; Li, G.; Gell, L.; Lin, S.; Tang, Z.; Häkkinen, H.; Zheng, N. An Intermetallic $Au_{24}Ag_{20}$ Superatom Nanocluster Stabilized by Labile Ligands. *J. Am. Chem. Soc.* **2015**, *137*, 4324–4327.
86. Wang, Y.; Wan, X.-K.; Ren, L.; Su, H.; Li, G.; Malola, S.; Lin, S.; Tang, Z.; Häkkinen, H.; Teo, B.K.; Wang, Q.-M.; Zheng, N. Atomically Precise Alkynyl-Protected Metal Nanoclusters as a Model Catalyst: Observation of Promoting Effect of Surface Ligands on Catalysis by Metal Nanoparticles. *J. Am. Chem. Soc.* **2016**, *138*, 3278–3281.
87. Zeng, J.-L.; Guan, Z.-J.; Du, Y.; Nan, Z.-A.; Lin, Y.-M.; Wang, Q.-M. Chloride-Promoted Formation of a Bimetallic Nanocluster $Au_{80}Ag_{30}$ and the Total Structure Determination. *J. Am. Chem. Soc.* **2016**, *138*, 7848–7851.
88. Lei, K.; Wan, X.-K.; Yuan, S.-F.; Guan, Z.-J. Alkynyl Approach toward the Protection of Metal Nanoclusters. *Acc. Chem. Res.* **2018**, *51*, 2465–2474.
89. MZhang, M.; Dong, X.-Y.; Wang, Y.-J.; Zang, S.-Q.; Mak, T.C.W. Recent progress in functional atom-precise coinage metal clusters protected by alkynyl ligands. *Coord. Chem. Rev.* **2022**, *453*, 214315.
90. Hopkinson, M.N.; Richter, C.; Schedler, M.; Glorius, F. An overview of N-heterocyclic carbenes. *Nature* **2014**, *510*, 485–496.
91. Zhou, Y.B.; Chen, W.Z. Synthesis and characterization of square-planar tetranuclear silver and gold clusters supported by a pyrazole-linked bis(N-heterocyclic carbene) ligand. *Organometallics* **2007**, *26*, 2742–2746.
92. Vignolle, J.; Tilley, T.D. N-Heterocyclic carbene-stabilized gold nanoparticles and their assembly into 3D superlattices. *Chem. Commun*. **2009**, *46*, 7230–7232.
93. Kiefer, C.; Bestgen, S.; Gamer, M.T.; Lebedkin, S.; Kapes, M.M.; Roesky, P.W. Alkynyl-functionalized gold NHC complexes and their coinage metal clusters. *Dalton Trans.* **2015**, *44*, 13662–13670.
94. Scherbaum, F.; Groohmann, A.; Huber, B.; Krüger, C.; Schmidbauer, H. Aurophilicity as a Consequence of Relativistic Effects: The Hexakis(triphenylphosphaneaurio) methane Dication $[(Ph_3PAu)_6C]^{2\oplus}$. *Angew. Chem. Int. Ed.* **1988**, *27*, 1544–1546.
95. Gabbaï, F.P.; Scheir, A.; Riede, J.; Scmidbauer, H. Synthesis of the Hexakis [(triphenylphosphane)gold(I)]methanium(2+) Cation from Trimethylsily ldiazomethane; Crystal Structure Determination of the Tetrafluoroborate Salt. *Chem. Ber.* **1997**, *130*, 111–114.
96. Ube, H.; Zhang, Q.; Shinoya, M. A Carbon-Centered Hexagold(I) Cluster Supported by *N*-Heterocyclic Carbene Ligands. *Organometallics* **2018**, *37*, 2007–2009.
97. Lei, Z.; Pei, N.-L.; Ube, H.; Shionoya, M. Reconstituting C-centered hexagold (I) clusters with N-heterocyclic carbene ligands. *Bull. Chem. Soc. Jpn.* **2021**, *94*, 1324–1330.
98. Wei, J.; Halet, J.-F.; Kahlal, S.; Saillard, J.-Y.; Munoz-Castro, A. Toward the Formation of *N*-Heterocyclic-Carbene-Protected Gold Clusters of Various Nuclearities. A Comparison with Their Phosphine-Protected Analogues from Density Functional Theory Calculations. *Inorg. Chem*. **2020**, *59*, 15240–15249.

99. Robilotto, T.J.; Bacsa, J.; Gray, T.G.; Sadighi, J.P. Synthesis of a Trigold Monocation: An Isolobal Analogue of $[H_3]^+$. *Angew. Chem. Int. Ed.* **2012**, *51*, 12077–12080.
100. Jin, L.; Weinberger, D.S.; Melaimi, M.; Moore, C.E.; Rheingold, A.L.; Bertrand, G. Trinuclear Gold Clusters Supported by Cyclic (alkyl)(amino)carbene Ligands: Mimics for Gold Heterogeneous Catalysts. *Angew. Chem., Int. Ed.* **2014**, *53*, 9059–9063.
101. Narouz, M.R.; Takano, S.; Lummis, P.A.; Levchenko, T.I.; Nazemi, A.; Kaappa, S.; Malola, S.; Yousefalizadeh, G.; Calhoun, L.A.; Stamplecoskie, K.G.; Häkkinen, H.; Tsukuda, T.; Robust, C.M. Highly Luminescent Au_{13} Superatoms Protected by *N*-Heterocyclic Carbenes. *J. Am. Chem. Soc.* **2019**, *141*, 14997–15002.
102. Shen, H.; Deng, G.; Kaappa, S.; Tan, T.; Han, Y.-Z.; Malola, S.; Lin, S.-C.; Teo, B.; Häkkinen, K.; Zheng, H.N. Highly Robust but Surface-Active: An *N*-Heterocyclic Carbene Stabilized Au_{25} Nanocluster. *Angew. Chem. Int. Ed.* **2019**, *58*, 17731–17735.
103. Albright, E.L.; Levcheko, T.I.; Kulkarni, V.K.; Sullivan, A.I.; De Jesus, J.F.; Malola, S.; Takano, S.; Nambo, M.; Stamplekoskie, K.; Häkkinen, H.; Tsukuda, T.; Crudden, C.M. N-Heterocyclic Carbene-Stabilized Atomically Precise Metal Nanoclusters, *J. Am. Chem. Soc*. **2024**, *146*, 5759–5780.
104. Shen, H.; Xiang, S.; Xu, Z.; Liu, C.; Li, X.; Sun, C.; Lin, S.; Teo, B.K.; Zheng, N. Superatomic Au_{13} clusters ligated by different N-heterocyclic carbenes and their ligand-dependent catalysis, photoluminescence, and proton sensitivity. *Nano Res.* **2020**, *13*, 1908–1911.
105. Sun, J.; Tang, X.; Tang, J.; Zhang, Y.S.; Li, Z.; Cholumen; Guo, S.; Shen, H. Simple Approach toward *N*-Heterocyclic Carbene-Protected Gold Nanoclusters. *Inorg. Chem.* **2023**, *62*, 5088–5094.
106. McPartlin, M.; Mason, R.; Malatesta, L. Novel cluster complexes of gold (0)-gold (I). *J. Chem. Soc. D* **1969**, *7*, 334.
107. Adnan, R.H.; Madridejos, J.M.L.; Alotabi, A.S.; Metha, G.F.; Andersson, G.G. A Review of State of the Art in Phosphine Ligated Gold Clusters and Application in Catalysis. *Adv. Sci.* **2022**, *9*, 2105692.
108. Mingos, D.M.P. Gold–A flexible friend in molecular chemistry. *J. Chem. Soc. Dalton Trans.* **1996**, *5*, 561–566.
109. Mingos, D.M.P. Structural and bonding pattern in gold clusters. *J. Chem. Soc. Dalton Trans.* **2015**, *44*, 6680–6695.
110. Ligare, M.R.; Johnson, G.E.; Laskin, J. Observing the real time formation of phosphine-ligated gold clusters by electrospray ionization mass spectrometry. *Phys. Chem. Chem. Phys.* **2017**, *19*, 17187.
111. Pettibone, J.M.; Reardon, N.R. Nucleation products of ligated nanoclusters unaffected by temperature and reducing agent. *Nanoscale* **2012**, *4*, 5593.
112. Kang, X.; Zhu, M.Z. Transformation of Atomically Precise Nanoclusters by Ligand-Exchange. *Chem. Mater.* **2019**, *31*, 24, 9939–9969.
113. Anderson, D.P.; Alvino, J.F.; Gentleman, A.; Qahtani, H.A.; Thomsen, L.; Polson, M.I.J.; Metha, G.F.; Golovko, V.B.; Andersson, G.G. Chemically Synthesised Atomically Precise Gold Clusters Deposited and Activated on Titania. *Phys. Chem. Chem. Phys.* **2013**, *15*, 3917–3929.
114. Schmid, G. Clusters and colloids-bridges between molecular and condensed materials. *Mater. Chem. Phys.* **1991**, *29*, 133–142.
115. Schmid, G.; Liu, Y.-P.; Schumann, M.; Raschke, T.; Radehaus, C. Quasi One-Dimensional Arrangements of $Au_{55}(PPh_3)_{12}Cl_6$ Clusters and Their Electrical Properties at Room Temperature. *Nano Lett*. **2001**, *1*, 405–407.
116. Jian, N.; Stapelfeldt, C.; Hu, K.-J.; Fröba, M.; Palmer, R.E. Hybrid atomic structure of the Schmid cluster $Au_{55}(PPh_3)_{12}Cl_6$ resolved by aberration-corrected STEM. *Nanoscale* **2015**, *7*, 885–888.
117. Wen, F.; Englert, U.; Gutrath, B.; Simon, U. Electrochemical and Optical Properties of $[Au_9(PPh_3)_8](NO_3)_3$. *Eur. J. Inorg. Chem.* **2008**, *2008*, 106–111.
118. Gutrath, B.S.; Englert, U.; Wang, Y.; Simon, U. A Missing Link in Undecagold Cluster Chemistry: Single-Crystal X-ray Analysis of $[Au_{11}(PPh_3)_7Cl_3]$. *Eur. J. Inorg. Chem.* **2013**, *2013*, 2002–2006.
119. Gutrath, B.S.; Schiefer, F.; Homberger, M.; Englert, U.; Şerb, M.-D.; Bettray, W.; Beljakov, I.; Meded, V.; Wenzel, W.; Simon, U. Molecular and Electronic Structure of the Cluster $[Au_8(PPh_3)_8](NO_3)_2$. *Eur. J. Inorg. Chem.* **2016**, *2016*, 975–981.
120. McKenzie, L.C.; Zaikova, T.O.; Hutchison, J.E. Structurally similar triphenylphosphine-stabilized undecagolds, $Au_{11}(PPh_3)7Cl_3$ and $[Au_{11}(PPh_3)8Cl_2]$ Cl, exhibit distinct ligand exchange pathways with glutathione. *J. Am. Chem. Soc.* **2014**, *136*, 13426–13435.
121. Xiao, F.-X.; Hung, S.F.; Miao, J.W.; Wang, H.Y.; Yang, H.B.; Liu, B. Metal-Cluster-Decorated TiO_2 Nanotube Arrays: A Composite Heterostructure toward Versatile Photocatalytic and Photoelectrochemical Applications. *Small* **2015**, *11*, 554–567.
122. Liu, C.; Abroshan, H.; Yan, C.; Li, G.; Haruta, M. One-Pot Synthesis of $Au_{11}(PPh_2Py)_7Br_3$ for the Highly Chemoselective Hydrogenation of Nitrobenzaldehyde. *ACS Catal.* **2016**, *6*, 92–99.
123. Fernando, A.; Aikens, C.M. Ligand Exchange Mechanism on Thiolate Monolayer Protected $Au_{25}(SR)_{18}$Nanoclusters. *J. Phys. Chem. C* **2015***, 119,* 20179–20187.

124. Pengo, P.; Bazzo, C.; Boccalon, M.; Pasquato, L. Differential Reactivity of the Inner and Outer Positions of $Au_{25}(SCH_2CH_2Ph)_{18}$ Dimeric Staples under Place Exchange Conditions. *Chem. Commun*. **2015**, *51*, 3204–3207.
125. Kumara, C.; Aikens, C.M.; Dass, A. X-ray Crystal Structure and Theoretical Analysis of $Au_{25-x}Ag_x(SCH_2CH_2Ph)_{18}^-$. *Alloy J. Phys. Chem. Lett*. **2014**, *5*, 461–466.
126. Bose, P.; Roy, J.; Khokhar, V.; Mondal, B.; Natarajan, G.; Manna, S.; Yadav, V.; Yamijala, S.S.R.K.C.; Nyayban, A.; Nonappa; Pradeep, T. Interparticle Antigalvanic Reactions of Atomically Precise Silver Nanoclusters with Plasmonic Gold Nanoparticles: Interfacial Control of Atomic Exchange. *Chem. Mater*. **2024**, *6*, 7581–7594.
127. Shibu, E.S.; Muhammed, M.A.H.; Tsukuda, T.; Pradeep, T. Ligand exchange of $Au_{25}SG_{18}$ leading to functionalized gold clusters: Spectroscopy, kinetics, and luminescenc. *J. Phys. Chem. C* **2008**, *112*, 12168–12176.
128. Takano, S.; Hirai, H.; Muramatsu, S.; Tsukuda, T. Hydride-Doped Gold Superatom $(Au_9H)^{2+}$: Synthesis, Structure, and Transformation. *J. Am. Chem. Soc.* **2018**, *140*, 8380–8383.
129. Liao, C.; Zhu, M.Z.; Jiang, D.-E.; Li, X.S. Manifestation of the interplay between spin-orbit and Jahn-Teller effects in Au_{25} superatom UV-Vis. fingerprint spectra. *Chem. Sci*. **2023**, *14*, 4666–4671.
130. Pan, P.Y.; Zhang, L.D.; Wei, X.; Tian, Y.P.; Kang, X.; Zhang, Q.; Zhu, M.Z. Two-, and Three-Photon Excited Fluorescence of Atomically Precise Metal Nanoclusters. *Angew. Chem. Int. Ed*. **2022**, *61*, e202213016.
131. Kang, X.; Zhu, M.Z. Tailoring the photoluminescence of atomically precise nanoclusters, *Chem. Soc. Rev*. **2019**, *48*, 2422–2457.
132. Zhu, J.; Zhao, R.; Shen, H.L.; Zhu, C.; Zhou, M.; Kang, X.; Zhu, M.Z. Intramolecular Aggregation-Induced Surface Coupling of Metal Nanoclusters: Structure Elucidation and Photoluminescence Manipulation. *Agregate* **2025**, *6*, e720. https://doi.org/10.1002/agt2.720.
133. Goswami, N.; Yao, Q.; Luo, Z.; Li, J.; Chen, T.J. Luminescent Metal Nanoclusters with Aggregation-Induced Emission. *J. Phys. Chem. Lett*. **2016**, *7*, 962–975.
134. Wang, S.; Meng, X.; Das, A.; Li, T.; Song, Y.; Cao, T.; Zhu, X.; Zhu, M.; Jin, R. A 200-Fold Quantum Yield Boost in the Photoluminescence of Silver-Doped Ag_xAu_{25-x} Nanoclusters: The 13th Silver Atom Matters. *Angew. Chem. Int. Ed.* **2014**, *53*, 2376–2380.
135. Bootharaju, M.S.; Kozlov, S.M.; Cao, Z.; Shkurenko, A.; El-Zohry, A.M.; Mohammed, O.F.; Eddaoudi, M.; Bakr, O.M.; Cavallo, L.; Basset, J.-M. Tailoring the Crystal Structure of Nanoclusters Unveiled High Photoluminescence via Ion Pairing. *Chem. Mater.* **2018**, *30*, 2719–2725.
136. Ma, W.; Xu, L.G.; de Moura, A.; Wu, X.L.; Kuang, H.; Xu, C.L.; Kotov, N.A. Chiral inorganic nanostructures. *Chem. Rev.* **2017**, *117*, 8041–8093.
137. Chen, Y.X.; Zeng, C.J.; Liu, C.; Kirschbaum, K.; Gayathri, C.; Gil, R.R.; Rosi, N.L.; Jin, R.C. Crystal Structure of Barrel-Shaped Chiral Au_{130}(*p*-MBT)$_{50}$ Nanocluster. *J. Am. Chem. Soc*. **2015**, *137*, 10076-100079.
138. Dolamic, I.; Knoppe, S.; Dass, A.; Bürgi, T. First Enantioseparation and Circular Dichroism Spectra of Au_{38} Clusters Protected by Achiral Ligands. *Nat. Commun*. **2012**, *3*, 798.
139. Zeng, C.; Chen, Y.; Kirschbaum, K.; Appavoo, K.; Sfeir, M.Y.; Jin, R. Structural Patterns at All Scales in a Nonmetallic Chiral $Au_{133}(SR)_{52}$. *Sci. Adv.* **2015**, *1*, e1500045.
140. Shichibu, Y.; Ogawa, Y.; Sugiuchi, M.; Konishi, K. Chiroptical activity of Au_{13} clusters: Experimental and theoretical understanding of the origin of helical charge movements. *Nanoscale Adv.* **2021**, *3*, 1005–1011.
141. Masatake, H.; Tetsuhiko, K.; Hiroshi, S.; Nobumasa, Y.; Haruta, M. Novel Gold Catalysts for the Oxidation of Carbon Monoxide at a Temperature far Below 0 °C. *Chem. Lett.* **1987**, *16*, 405–408.
142. Okumura, M.; Kitagawa, Y.; Yamagcuhi, K.; Akita, T.; Tsubota, S.; Haruta, M. Direct Production of Hydrogen Peroxide from H_2 and O_2 over Highly Dispersed Au catalysts. *Chem. Lett*. **2003**, *32*, 822–823.
143. Pina, D.; Falletta, E.; Rossi, M. Update on selective oxidation using gold. *Chem. Soc. Rev.* **2012**, *41*, 350.
144. Chen, Y.; Liu, C.; Abroshan, H.; Li, Z.; Wang, J.; Li, G.; Haruta, M. One-Pot Synthesis of $Au_{11}(PPh_2Py)_7Br_3$ for the Highly Chemoselective Hydrogenation of Nitrobenzaldehyde. *J. Catal.* **2016**, *340*, 287.
145. Bond, G.C.; Thompson, D.T. Catalysis by gold. *Catal. Rev. Sci. Eng*. **1999**, *41*, 319–388.
146. Lu, F.; Ruiz, J.; Astruc, D. Nanoparticles as Recyclable Catalysts: The Fast-growing Frontier between Homogeneous and Heterogeneous Catalysts. *Angew. Chem. Int. Ed*. **2005**, *44*, 7852–7872.
147. Astruc, D. *Nanoparticles and Catalysis*; Wiley-VCH: Weinhein, Germany, 2007.
148. Ishida, T.; Murayama, T.; Taketoshi, A.; Haruta, M. Importance of Size and Contact Structure of Gold Nanoparticles for the Genesis of Unique Catalytic Processes. *Chem. Rev.* **2020**, *120*, 464–525.
149. Yamamoto, K.; Imaoka, T.; Tanabe, M.; Gambe, T. New Horizon of Nanoparticle and Cluster Catalysis with Dendrimers, *Chem. Rev*. **2020**, *120*, 1397–1437.
150. Astruc, D. Introduction: Nanoparticles in Catalysis. *Chem. Rev*. **2020**, *120*, 461–463.
151. Jin, R.C.; Li, G.; Sharma, S.; Li, Y.W.; Du, X.S. Toward Active-Site Tailoring in Heterogeneous Catalysis by Atomically Precise Metal Nanoclusters with Crystallographic Structures. *Chem Rev.* **2021**, *121*, 567–648.

152. Liu, Z.H.; Wu, Z.N.; Yao, Q.F.; Cao, Y.T.; Chai, Q.J.H.; Xie, J.P. Correlations between the fundamentals and applications of ultrasmall metal nanoclusters: Recent advances in catalysis and biomedical applications. *Nano Today.* **2021**, *36*, 101053.
153. Du, Y.; Sheng, H.; Astruc, D.; Zhu, M.Z. Atomically Precise Noble Metal Nanoclusters as Efficient Catalysts: A Bridge between Structure and Properties. *Chem. Rev*. **2020**, *120*, 526–622.
154. Yang, D.; Pei, W.; Zhou, S.; Zhao, J.; Ding, W.; Zhu, Y. Controllable Conversion of CO_2 on Non-Metallic Gold Clusters. *Angew. Chem. Int. Ed*. **2020**, *59*, 1919–1924.
155. Nie, X.; Qian, H.; Ge, Q.; Xu, H.; Jin, R. CO Oxidation Catalyzed by Oxide-Supported $Au_{25}(SR)_{18}$ Nanoclusters and Identification of Perimeter Sites as Active Centers. *ACS Nano* **2012**, *6*, 6014–6022.
156. Li, G.; Jin, R. Gold Nanocluster-Catalyzed Semihydrogenation: A Unique Activation Pathway for Terminal Alkynes. *J. Am. Chem. Soc*. **2014**, *136*, 11347–11354.
157. Li, G.; Jiang, D.-E.; Liu, C.; Yu, C.; Jin, R. Oxide-Supported Atomically Precise Gold Nanocluster for Catalyzing Sonogashira Cross-Coupling. *J. Catal*. **2013**, *306*, 177–183.
158. Kauffman, D.R.; Alfonso, D.; Matranga, C.; Qian, H.F.; Jin, R.C. Experimental and Computational Investigation of Au_{25} Clusters and CO_2: A Unique Interaction and Enhanced Electrocatalytic Activity. *J. Am. Chem. Soc*. **2012**, *134*, 10237–10243.
159. Seong, H.; Efremo, V.; Park, G.; Kim, H.; Joo, J.S.; Lee, D. Atomically Precise Gold Nanoclusters as Model Catalysts for Identifying Active Sites for Electroreduction of CO_2. *Angew. Chem.*, *Int. Ed*. **2021**, *60*, 14563–14570.
160. Narouz, M.R.; Osten, K.M.; Unsworth, P.J.; Man, R.W.Y.; Salorinne, K.; Takano, S.; Tomihara, R.; Kaappa, S.; Malola, S.; Dinh, C.T.; Padmos, J.D.; Ayoo, K.; Garrett, P.J.; Nambo, M.; Horton, J.H.; Sargent, E.H.; Häkkinen, H.; Tsukuda, T.; Crudden, C.M. N-heterocyclic carbene-functionalized magic-number gold nanoclusters*. Nat. Chem*. **2019**, *11*, 419–425.
161. Zhao, J.; Ziarati, A.; Bûrgi, T. Tuning Atomically Precise Gold Nanoclusters for Selective Electroreduction of CO_2. *Angew. Chem. Int. Ed*. **2025**, *64*, e202504320.
162. Wang, C.; Astruc, D. Nanogold plasmonic photocatalysis for organic synthesis and clean energy conversion. *Chem. Soc. Rev*. **2014**, *43*, 7188–7216.
163. Gellé, A.; Gin, T.; de la Garza, L.; Price, G.D.; Beistero, L.V.; Moores, A. Applications of Plasmon-Enhanced Nanocatalysis to Organic Transformations. *Chem. Rev*. **2020**, *120*, 986–1041.
164. Kang, N.; Wei, X.; Shen, R.; Li, B.; Cal, E.G.; Moya, S.; Salmon, L.; Wang, C.; Coy, E.; Berlande, M.; Pozzo, J.-L.; Astruc, D. Fast Au-Ni@ZIF-8-Catalyzed Ammonia Borane Hydrolysis Boosted by Dramatic Volcano-Type Synergy and Plasmonic Acceleration. *Appl. Catal. B* **2023**, *320*, 121957.
165. Zhao, Q.; Kang, N.; Moro, M.M.; Cal, E.G.; Moya, S.; Coy, E.; Salmon, L.; Liu, X.; Astruc, D. Sharp Volcano-Type Synergy and Visible-Light Acceleration in H_2 Release upon $B_2(OH)_4$ Hydrolysis Catalyzed by Au-Rh@click-dendrimer Nanozymes. *ACS Appl. Energy Mater.* **2022**, *5*, 3834–3844.
166. Wang, T.; Hamon, J.-R.; Wang, C. D. Astruc. Hydrogen production via nanocatalyzed ammonia borane hydrolysis: State of the art, recent progress and perspectives. *Coord. Chem. Rev*. **2025**, *541*, 216871.
167. Liang, H.; Chen, Q.; Mo, Q.-L.; Wu, Y.; Xiao, F.-X. Atomically precise thiolate-protected goldnanoclusters: Current advances in solar-powered photoredox catalysis. *J. Mater. Chem. A* **2023**, *11*, 9401–9426.
168. Kogo, A.; Sakai, N.; Tatsuma, T. Photocatalysis of Au_{25}-Modified TiO_2 under Visible and near Infrared Light. *Electrochem. Commun*. **2010**, *12*, 996–999.
169. Sakai, N.; Tatsuma, T. Photovoltaic Properties of Glutathione-Protected Gold Clusters Adsorbed on TiO_2 Electrodes. *Adv. Mater*. **2010**, *22*, 3185–3188.
170. Li, T.; Zhang, R.R.; Fang, N.J.; Shi, Y.B.; Li, J.H.; He, C.S.; Chu, Y.H. Metal cluster-mediated photocatalysis: Synthesis; characterization; application. *Nanoscale* **2025**, *17*, 9834–9869.
171. Zeng, Z.H.; Xiao, F.X.; Xu, Y.J. Atomically Precise Alloy Nanoclusters Steering Photocatalysis. *Small* **2025**, *21*, 2505282.
172. Labande, A.; Ruiz, J.; Astruc, D. Supramolecular Gold Nanoparticles for the Redox Recognition of Oxoanions: Syntheses, Titrations, Stereoelectronic Efects, and Selectivity. *J. Am. Chem. Soc*. **2002**, *124*, 1782–1789.
173. Muhammed, M.A.; Verma, P.K.; Pal, S.K.; Kumar, R.C.; Paul, S.; Omkumar, R.V.; Bright, T.B.P. Nir-Emitting Au_{23} from Au_{25}: Characterization and Applications Including Biolabeling, *Chem. Eur. J.* **2009**, *15*, 10110–10120.
174. Zheng, J.; Zhou, C.; Yu, M.X.; Liu, J.B. Different Sized Luminescent Gold Nanoparticles. *Nanoscal*e **2012**, *4*, 4073–4083.
175. Tan, X.; Jin, R. Ultrasmall Metal Nanoclusters for Bio-Related Applications. *Nanomed. Nanobiotechnol*. **2013**, *5*, 569–581.
176. Yuan, X.; Luo, Z.; Yu, Y.; Yao, Q.; Xie, J. Luminescent Noble Metal Nanoclusters as an Emerging Optical Probe for Sensor Development. *Chem. Asian J.* **2013**, *8*, 858–871.

177. Wang, S.; Zhu, X.Y.; Cao, T.T.; Zhu, M.Z. A simple model for understanding the fluorescence behavior of Au_{25} nanoclusters. *Nanoscale* **2014**, *6*, 5777–5781.
178. Zhang, L.B.; Wang, E.K. Metal nanoclusters: New fluorescent probes for sensors and bioimaging. *Nano Today* **2014**, *9*, 132–157.
179. Zhang, X.-D.; Luo, Z.; Chen, J.; Shen, X.; Song, S.; Sun, Y.; Fan, S.; Fan, F.; Leong, D.T.; Xie, J. Ultrasmall $Au_{10–12}(SG)_{10–12}$ Nanomolecules for High Tumor Specificity and Cancer Radiotherapy *Adv. Mater*. **2014**, *26*, 4565–4568.
180. He, L.Z.; Dong, T.T.; Jiang, D.E.; Zhang, Q.C. Recent progress in atomically precise metal nanoclusters: From bio-related properties to biological applications. *Coord. Chem. Rev*. **2025**, *535*, 216633.
181. Sullivan, A.I.; Steele, E.A.; Takano, S.; Zeinizade, E.; Chen, J.; Malola, S.; Siddhant, K.; Häkkinen, H.; Stamplecoskie, K.G.; Tsukuda, T.; Zheng, G.; Crudden, C.M. Diving into Unknown Waters: Water-Soluble Clickable Au_{13}Nanoclusters Protected with N-Heterocyclic Carbenes for Bio-Medical Applications. *J. Am. Chem. Soc.* **2025**, *147*, 4230–4238.
182. Gallud, A.; Delaval, M.; Kinaret, P.A.S.; Marwa, V.S.; Fortino, V.; Ytterberg, J.; Zubarev, R.; Skoog, T.; Kere, J.; Correia, M.; Löchner, K.; Al-Ahmady, Z.; Kostarelos, K.; Ruiz, J.; Astruc, D.; Monopoli, M.; Moya, S.; Savolainen, K.; Alenius, H.; Tau, D.G.; Fadeel, B. Multi-Parametric Profiling of Engineered Nanomaterials: Unmasking the Surface Coating Effect. *Adv. Sci*. **2020**, *7*, 2002221.
183. Pan, Y.; Neuss, S.; Leifert, A.; Fischler, M.; Wen, F.; Simon, U.; Schmid, G.; Brandau, W.; Jahnen-Dechent, W. Size-dependent cytotoxicity of gold nanoparticles. *Small* **2007**, *3*, 1941–1949.
184. Li, H.; Kang, X.; Zhu, M.Z. Nanocluster-based aggregates: Assembled forms, driving forces, and structure-related properties. *Coord. Chem. Rev.* **2025**, *539*, 216738.
185. Sethumadhavan, V. Nonappa, Atomically precise noble metal nanoclusters for engineering self-assembled two-dimensional materials. *Dalton Trans*. **2025**, *54*, 11770–11789.
186. Nahan, E.N.; Aparna, R.K.; Chandrashekar, P.; Alam, N.; James, G.; Mandal, S. Ligand engineering for designing atomically precise metal nanoclusters and cluster-assemblies for potential applications. *J. Chem. Sci.* **2025**, *137*, 46.
187. Yonesato, K.; Yanai, D.; Yamaguchi, K.; Suzuki, K. Recent Advances in Polyoxometalate-Metal Nanocluster Hybrids. *Chem. Eur. J.* **2025**, *31*, e202500877.
188. Huang, J.H.; Cui, Y.; Wang, Z.Y.; Zang, S.-Q. Carborane Meets Metal Nanocluster: New Opportunities in Nanomaterials. *Acc. Chem. Res.* **2025**, *58*, 1249–1261.
189. Barik, S.K.; Rao, M.S.K.; Jali, B.R.; Halet, J.-F.; Jena, H.S. Helical self-assemblies of molecular-like coinage metal nanoclusters assemblies and their emerging applications. *Coord. Chem. Rev*. **2025**, *525*, 216341.
190. Zeng, L.L.; Zhou, M.; Jin, R.C. Evolution of Excited-State Behaviors of Gold Complexes, Nanoclusters and Nanoparticles. *ChemPhysChem* **2024**, *25*, e202300687.
191. Zhu, H.G.; Wang, Z.P.; Yao, Q.F.; Zhang, Z.P.; Yao, Q.F.; Zhang, P.; Xie, J.P.; Yuan, X. Metal Nanoclusters for Cancer Imaging and Treatment. *Adv. Funct. Mater.* **2025**, *35*, e07924.
192. Zheng, Y.K.; Wu, J.B.; Jiang, H.; Wang, X.M. Gold nanoclusters for theranostic applications. *Coord. Chem. Rev.* **2021**, *431*, 213689.
193. Singh, J.; Alruwaili, N.K.; Aodah, A.; Almalki, W.H.; Almujri, S.S.; Alrobaian, M.; Rab, S.O.; Alanezi, A.A.; Haji, E.M.; Barkat, A. Gold nanoclusters in cancer drug delivery: Advances and emerging applications. *J. Drug. Deliv. Sci. Technol*. **2025**, *105*, 106594.
194. Sarkar, S.; Das, J.; Debnath, B.; Ramzan, M.; Ashique, S.; Taghizadeh-Hesary, F. Nanobubbles: An emerging therapeutic paradigm for targeted cancer therapy. *Bioinorg. Chem.* **2025**, *164*, 108927.
195. Sun, J.Q.; Cheng, W.V.; Liu, X.; Xiang, H.X.; Ruan, C.H.; Chen, F.Z.; Yao, C.H. Gold clusters: A promising NIR-II probe for bioimaging and biosensing. *Coord. Chem. Rev.* **2025**, *533*, 216544.
196. Baghdasaryan, A.; Dai, H. Molecular Gold Nanoclusters for Advanced NIR-II Bioimaging and Therapy. *Chem. Rev.* **2025**, *125*, 5195–5227.
197. Lu, T.Y.; Dong, J.X.; Li, Y.L.; Wang, J.J.; Su, M.; Fan, Y.J.; Shen, S.G.; Gao, Z.F. 0D Fluorescent Nanomaterials: Preparation, Properties, and its Antibacterial Applications. *Adv. Nanobiomed. Res.* **2025**, 2500110. https://doi.org/10.1002/anbr.202500110.
198. Gao, Y.X.; Kang, J.; Tian, H.Y.; Dong, A. Gold nanoparticle-based antibacterial materials and bioapplications. *Soft Matter.* **2025**, *21*, 6832–6851.
199. Zhao, Y.; Zhou, H.M.; Qiao, L.L.; Ye, H.F.; Xu, J.M.; Antoine, R.; Deng, L.H.; Zhang, S.J.; Ye, H.F. Tumor-targeted ratiometric fluorescent gold nanoclusters for monitoring apoptosis and quantifying pH in vivo. *Sens. Act. B Chem.* **2025**, *444*, 138357.
200. Guan, Z.J.; Li, J.J.; Hu, F.; Wang, Q.M. Structural Engineering toward Gold Nanocluster Catalysis. *Angew. Chem. Int. Ed.* **2022**, *61*, e20220972.
201. Liu, X.; Cai, X.; Zhu, Y. Catalysis Synergism by Atomically Precise Bimetallic Nanoclusters Doped with Heteroatoms. *Acc. Chem. Res*. **2023**, *56*, 1528–1538.

202. Wang, M.Y.; Chen, Y.; Tang, C. Recent Advances in Ligand Engineering for Gold Nanocluster Catalysis: Ligand Library, Ligand Effects and Strategies. *Chem. Asian J.* **2023**, *18*, e202300463.
203. Yang, J.L.; Peng, Y.; Jia, Q.; Metal nanocluster-based hybrid nanomaterials: Fabrication and application. *Coord. Chem. Rev.* **2022**, *456*, 214391.
204. Jing, W.T.; Shen, H.; Qin, R.X.; Wu, Q.Y.; Liu, K.L.; Zheng, N.F. Surface and Interface Coordination Chemistry Learned from Model Heterogeneous Metal Nanocatalysts: From Atomically Dispersed Catalysts to Atomically Precise Clusters. *Chem. Rev.* **2023**, *123*, 5948–6002.
205. Zhao, J.T.; Ziarati, A.; Rosspeintner, A.; Bürgi, T. Anchoring of Metal Complexes on Au_{25} Nanocluster for Enhanced Photocoupled Electrocatalytic CO_2 Reduction. *Angew. Chem. Int. Ed.* **2024**, *63*, e202316649.
206. Du, Y.X.; Fang, Y.; Wang, P.; Zhu, M.Z. Synergistic effects of atomically precise Au-based bimetallic nanocluster on energy-related small molecule catalysis. *Chem. Sci.* **2025**, *16*, 10642–10664.
207. Du, Y.X.; Wang, P.; Fang, Y.; Zhu, M.Z. Asymmetric Charge Distribution in Atomically Precise Metal Nanoclusters for Boosted CO_2 Reduction Catalysis. *ChemSusChem.* **2025**, *18*, e202402085.
208. Xia, N.; Wang, W.; Zhuang, S.I.; Gu, W.M.; Li, J.; Deng, H.T.; Wang, Y.B.; Wu, Z.K. Electrochemical Carbon Dioxide Reduction Reaction or Hydrogen Evolution Reaction: Kernel and Type-Dependent Catalytic Activity of Staples in Metal Nanoclusters. *Adv. Funct. Mater.* **2025**, *35*, 2507721.
209. Antoine, R.; Broyer, M.; Dugourd, P. Metal nanoclusters: From fundamental aspects to electronic properties and optical applications. *Sci. Technol*. *Adv. Mater*. **2023**, *24*, 2222546.
210. Jameel, M.S.; Wahab, H.A.; Ahmad, W.; Mehrdel, B.; Alanezi, S.T.; Khaniabadi, P.M.; Deyab, M.A. Inorganic nanoparticles as smart carriers for docetaxel delivery in cancer therapy: Mechanisms, targeting strategies, and translational insights. *J. Drug. Deliv. Sci. Technol*. **2025**, *114*, 107464.
211. Amiens, C.; Axet, M.R.; Igau, A.; Morales, E.M.; Philippot, K.; Romero, N.; Sutra, P. Metal complexes–metal nanoparticles hybrid systems, *Coord. Chem. Rev*. **2026**, *547*, 217053.
212. Gauffre, F.; Coppel, Y.; Marty, J.D.; Mingotaud, C.; Kahn, M. When coordination chemistry meets soft matter: From hybrid nanoparticles to assemblies. *Coord. Chem. Rev*. **2025**, *543*, 216893.
213. Hang, Y.J.; Wang, A.Y.; Wu, N.Q. Plasmonic silver and gold nanoparticles: Shape- and structure-modulated plasmonic functionality for point-of-caring sensing, bio-imaging and medical therapy, *Chem. Soc. Rev*. **2024**, *53*, 2932–2971.
214. Liu, L.C.; Corma, A. Metal Catalysts for Heterogeneous Catalysis: From Single Atoms to Nanoclusters and Nanoparticles. *Chem. Rev*. **2018**, *118*, 4981–5079.
215. Yang, H.C.; Duan, D.F.; Zhuang, Z.C.; Luo, Y.W.; Chen, J.; Xiong, Y.L.; Liu, X.W.; Wang, D.S. Understanding the Dynamic Evolution of Active Sites among Single Atoms, Clusters, and Nanoparticles. *Adv. Mater*. **2025**, *37*, 2415265.
216. Wei, J.Y.; Kahlal, S.; Halet, J.-F.; Munoz-Castro, A.; Saillard, J.-Y. Ligand-Induced Cuboctahedral versus Icosahedral Core Isomerism within Eight-Electron Heterocyclic-Carbene-Protected Gold Nanoclusters. *Inorg. Chem*. **2022**, *61*, 8623–8628.
217. Bühler, R.; Schütz, M.; Andriani, K.F.; Quiles, M.G.; de Mendonca, J.P.A.; Ocampo-Restrepo, V.K.; Stephan, J.; Ling, S.P.; Kahlal, S.; Saillard, J.-Y.; Gemel, C.; Da Silva, J.L.F.; Fischer, R.A. A living library concept to capture the dynamics and reactivity of mixed-metal clusters for catalysis. *Nat. Chem*. **2025**, *17*, 525–531.
218. Shi, W.Q.; Zheng, L.L.; He, R.L.; Han, X.S.; Guan, Z.J.; Zhou, M.; Wang, Q.M. Near-unity NIR phosphorescent quantum yield from a room-temperature solvated metal nanocluster. *Science* **2024**, *383*, 326-330.
219. Fang, F.; Zhu, N.S.Q.; Yao, Q.F.; Hu, W.P. Asymmetric catalysis promoted by hierarchical chirality of metal nanoclusters. *Sci. China-Mater*. **2025**, *68*, 3075–3092.
220. Kim, S.; Jääskö, H.; Park, K.C.; Malola, S.; Häkkinen, H.; Park, S.S. Tuning the Electrical Properties through Metal-Ion-Mediated Assembly in Au_{25} Nanocluster-Based Frameworks. *J. Am. Chem. Soc*. **2025**, *147*, 30803–30808.